# Terrestrial ecosystem carbon flux estimated using GOSAT and OCO-2 $XCO_2$ retrievals

Hengmao Wang[1], Fei Jiang[1,2*], Jun Wang[1], Weimin Ju[1], Jing M. Chen[1,3]

*1 Jiangsu Provincial Key Laboratory of Geographic Information Science and Technology, International Institute for Earth System Science, Nanjing University, Nanjing, 210023, China*
*2 Jiangsu Center for Collaborative Innovation in Geographical Information Resource Development and Application, Nanjing, 210023, China*
*3, Department of Geography, University of Toronto, Toronto, Ontario M5S3G3, Canada*

## Abstract

In this study, both the Greenhouse Gases Observing Satellite (GOSAT) and the Orbiting Carbon Observatory 2 (OCO-2) $XCO_2$ retrievals produced by NASA Atmospheric $CO_2$ Observations from Space (ACOS) project (Version b7.3), are assimilated within the GEOS-Chem 4D-Var assimilation framework to constrain the terrestrial ecosystem carbon flux during Oct 1, 2014 to Dec 31, 2015. One inversion for the comparison, using in situ $CO_2$ observations, and another inversion as a benchmark for the simulated atmospheric $CO_2$ distributions of the real inversions, using global atmospheric $CO_2$ trend and referred as poor-man inversion, are also conducted. The estimated global and regional carbon fluxes for 2015 are shown and discussed. $CO_2$ observations from surface flask sites and $XCO_2$ retrievals from TCCON sites are used to evaluate the simulated concentrations with the posterior carbon fluxes. Globally, the terrestrial ecosystem carbon sink (excluding biomass burning emissions) estimated from GOSAT data is stronger than that inferred from OCO-2 data, weaker than the in situ inversion, and matches the poor-man inversion to be the best. Regionally, in most regions, the land sinks inferred from GOSAT data are also stronger than those from OCO-2 data, and in North America, Asia, Europe, the carbon sinks inferred from GOSAT inversion are comparable to those from in situ inversion. For the latitudinal distribution of land sinks, the satellites-based inversions suggest a smaller boreal and tropical sink, but larger temperate sinks in both Northern and

* Corresponding author: Tel.: +86-25-83597077; Fax: +86-25-83592288; E-mail address: jiangf@nju.edu.cn

Southern Hemispheres than the in situ inversion. However, OCO-2 and GOSAT generally do not agree on which continent contains the smaller or larger sinks. Evaluations using flask and TCCON observations and the comparisons with in situ and poor-man inversions suggest that only GOSAT and the in situ inversions perform better than a poor-man's solution. GOSAT data can effectively improve the carbon flux estimates in Northern Hemisphere, while OCO-2 data, with the specific version used in this study, shows only slight improvement. The differences of inferred land fluxes between GOSAT and OCO-2 inversions in different regions are mainly related to the spatial coverage, the data amount, and the biases of these two satellites $XCO_2$ retrievals.

**Keywords**: Terrestrial ecosystem carbon flux, inversion, GOSAT, OCO-2, GEOS-Chem

## 1. Introduction

Atmospheric inverse modeling is an effective method for quantifying surface carbon fluxes at global and regional scales using the gradient of $CO_2$ measurements. Inversion studies based on in situ $CO_2$ observations agree well on global carbon budget estimates but differ greatly on regional carbon flux estimates and the partitioning of land and ocean fluxes as well, mainly due to the sparseness of observations in tropics, southern hemisphere oceans and the majority of continental interiors such as those in South America, Africa, and Boreal Asia (Peylin el al., 2013). Satellite observations offer an attractive means to constrain atmospheric inversions with their extensive spatial coverage over remote regions. Studies have shown that, theoretically, satellite observations, though with lower precision than in situ measurements, can improve the carbon flux estimates (Rayner and O Brien, 2001; Pak and Prather, 2001; Houweling et al., 2004; Baker et al., 2006; Chevallier et al., 2007; Miller et al., 2007; Kadygrov et al., 2009; Hungershoefer et al., 2010).

Satellite sensors designed specifically to retrieve atmospheric $CO_2$ concentrations, have been in operation in recent years. The Greenhouse Gases Observing Satellite (GOSAT) (Kuze et al., 2009), being the first satellite mission dedicated to observing $CO_2$ from space, was launched in 2009. The

National Aeronautics and Space Administration (NASA) launched the Orbiting Carbon Observatory 2 (OCO-2) satellite in 2014 (Crisp et al., 2017; Eldering et al., 2017). China's first $CO_2$ monitoring satellite (TanSat) was launched in 2016 (Wang et al., 2017; Yang et al., 2017). These satellites measure near-infrared sunlight reflected from the surface in $CO_2$ spectral bands and the $O_2$ A-band to retrieve column-averaged dry-air mole fractions of $CO_2$ ($XCO_2$), aiming to improving the estimation of spatial and temporal distributions of carbon sinks and sources. A number of inversions have utilized GOSAT $XCO_2$ retrievals to infer surface carbon fluxes (Basu et al., 2013; Maksyutov et al., 2013; Saeki et al., 2013; Chevallier et al., 2014; Deng et al., 2014; Houweling et al., 2015; Deng et al, 2016). Although large uncertainty reductions were achieved for regions which are under-sampled by in situ observations, these studies didn't give robust regional carbon flux estimates. There are large spreads in regional flux estimates in some regions among these inversions. Furthermore, regional flux distributions inferred from GOSAT $XCO_2$ data are significantly different from those inferred from in situ observations. For instance, several studies using GOSAT retrievals reported a larger than expected carbon sink in Europe (Basu et al., 2013; Chevallier et al., 2014; Deng et al., 2014; Houweling et al., 2015). The validity of this large Europe carbon sink derived from GOSAT retrievals is in intense debate and efforts to improve the accuracy of Europe carbon sink estimate are still ongoing (Reuter et al., 2014; Feng et al., 2016; Reuter et al., 2017).

Compared with GOSAT, OCO-2 has a higher sensitivity to column $CO_2$, much finer footprints and more extended spatial coverage, and thus has the potential to better constrain the surface carbon fluxes (Eldering et al., 2017). Studies have used OCO-2 $XCO_2$ data to estimate carbon flux anomalies during recent El Nino events (Chatterjee et al., 2017; Patra et al., 2017; Heymann et al., 2017; Liu et al., 2017). Nassar et al. (2017) applied OCO-2 $XCO_2$ data to infer emissions from large power plants. Miller et al. (2018) evaluated the potential of OCO-2 $XCO_2$ data in constraining regional biospheric $CO_2$ fluxes and found that in the current state of development, OCO-2 observations can only provide a reliable constraint on $CO_2$ budget at continental and hemispheric scales. At

present, it is still not clear whether with the improved monitoring capabilities and better spatial coverage, current OCO-2 observations have a greater potential than GOSAT observations for estimating $CO_2$ flux at regional or finer scale, since the biases also affect the usefulness of satellite retrievals greatly. It is therefore important to investigate how current OCO-2 $XCO_2$ data differ from GOSAT $XCO_2$ data in constraining carbon budget.

In this study, we evaluate the performance of GOSAT and OCO-2 $XCO_2$ data in constraining terrestrial ecosystem carbon flux. GOSAT and OCO-2 $XCO_2$ retrievals produced by the NASA Atmospheric $CO_2$ Observations from Space (ACOS) team are applied to infer monthly terrestrial ecosystem carbon sinks and sources from Oct, 2014 through December, 2015, using a 4D-Var scheme based on the GEOS-Chem Adjoint model (Henze et al., 2007). For comparisons, one inversion based on in situ measurements is conducted, and another simple one, which uses the global $CO_2$ trend as a benchmark for the simulated atmospheric $CO_2$ distributions of the real inversion, is also implemented. For simplicity, four inversions are referred as OCO-2 inversion, GOSAT inversion, in situ inversion and poor-man inversion, respectively. Inversion results are evaluated against surface flask $CO_2$ observations and Total Carbon Column Observing Network (TCCON) $XCO_2$ retrievals. This paper is organized as follows. Section 2 briefly introduces GOSAT and OCO-2 $XCO_2$ retrievals, surface observations and the inversion methodology. Inversion settings are described in Section 3. Results and discussions are presented in Section 4, and Conclusions are given in Section 5.

## 2. Data and Method

### 2.1 GOSAT and OCO-2 $XCO_2$ retrievals

Developed jointly by the National Institute for Environmental Studies (NIES), the Japanese Space Agency (JAXA) and the Ministry of the Environment (MOE) of Japan, GOSAT was designed to retrieve total column abundances of $CO_2$ and $CH_4$. The satellite flies at a 666 km altitude in a sun-synchronous orbit with 98° inclination that crosses the equator at 12:49 local time. It covers the whole globe in three days and has a footprint of 10.5 $km^2$ at nadir. OCO-2 is NASA's first

mission dedicated to retrieving atmospheric $CO_2$ concentration. It flies at 705 km altitude in a sun-synchronous orbit with an overpass time at approximately 13:30 local time and a repeat cycle of 16 days. Its grating spectrometer measures reflected sunlight in three near-infrared regions (0.765, 1.61 and 2.06 μm) to retrieve $XCO_2$. OCO-2 has a footprint of 1.29×2.25 $km^2$ at nadir and acquires eight cross-track footprints creating a swath width of 10.3 km.

Both GOSAT and OCO-2 $XCO_2$ products were created using the same retrieval algorithm, which is based on a Bayesian optimal estimation approach (Rogers et al., 2000; O Dell et al., 2011). The GOSAT and OCO-2 $XCO_2$ data used in this study are Version 7.3 Level 2 Lite products at the pixel level. The $XCO_2$ data from lite products are bias-corrected (Wunch et al., 2011). Before being used in our inversion system, the data are processed in three steps. First, the retrievals for the glint soundings over oceans have relatively larger uncertainty, thus the data over oceans are not used in our inversions (Wunch et al., 2017). Second, in order to achieve the most extensive spatial coverage with the assurance of using best quality data available, the $XCO_2$ data are filtered with two parameters, namely warn_levels and xco2_quality_flag, which are provided along with the $XCO_2$ data. All data with xco2_quality_flag not equaling 0 are removed, the rest are divided into three groups according the value of warn_levels, namely group 1, group 2 and group 3. In group 1, the warn_levels are less than 8, in group 2, the warn_levels are greater than 9 and less than 12, and in group 3, those are greater than 13. Group 1 has the best data quality, followed by group 2, and group 3 is the worst. Third, the pixel data are averaged within the grid cell of 2°×2.5°, which is the resolution of the global atmospheric transport model used in this study. In each grid of 2°×2.5°, only the groups of best data quality are selected and then averaged. The other variables like column averaging kernel, retrieval error and so on which are provided along with the $XCO_2$ product are also dealt with the same method. Figures 1a and 1b show the coverages and data amount of GOSAT and OCO-2 $XCO_2$ data during the study period after processing. The filtered GOSAT and OCO-2 retrievals are not evenly distributed spatially. Due to the cloud contamination, there are few retrievals in a large

portion of tropical land. In northern high latitude area, especially in boreal regions, due to the low soar zenith angle, available satellite retrievals are very sparse.

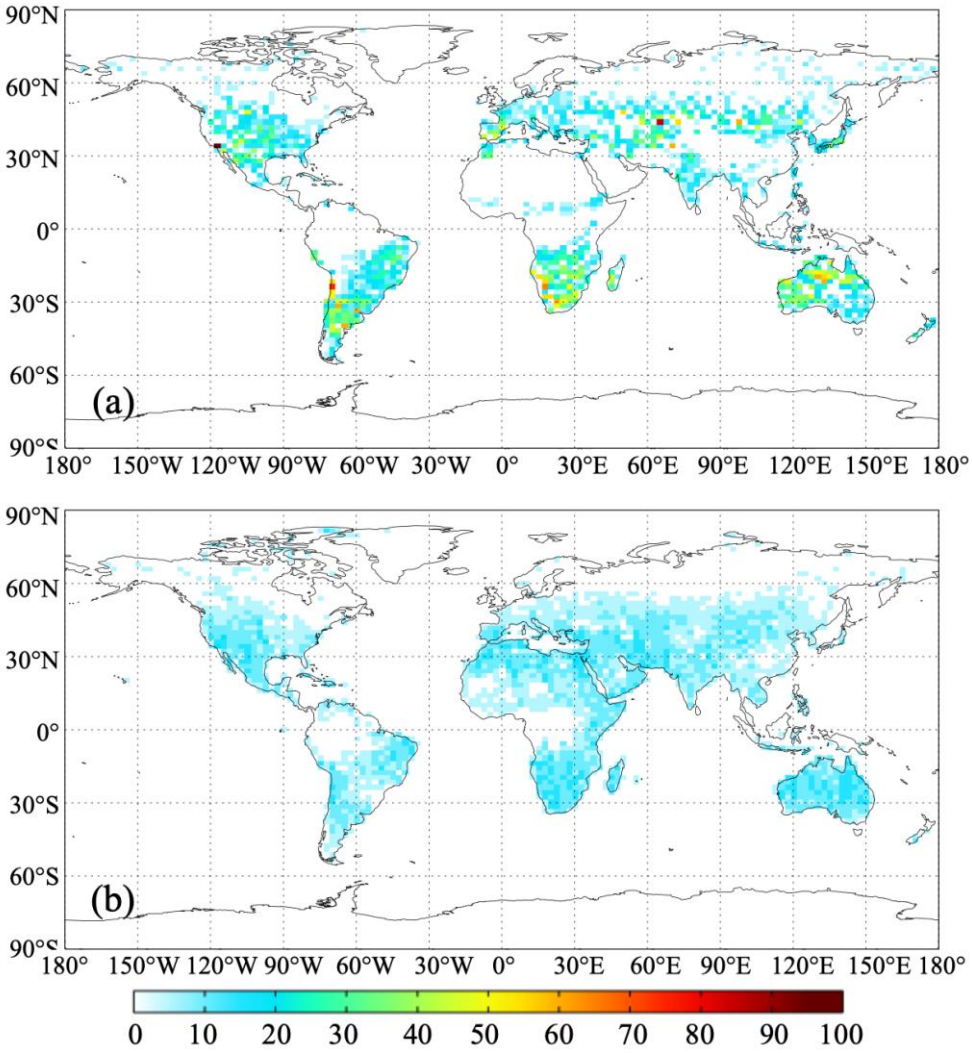


**Figure 1**. Data amount of each grid cell (2°×2.5°) of ACOS $XCO_2$ used in this study (a, GOSAT; b, OCO-2)

## 2.2 Surface observations and TCCON $XCO_2$ retrievals

Surface $CO_2$ observations are from the obspack_co2_1_CARBONTRACKER_CT2016_2017-02-06 product (ObsPackCT2016) (CarbonTracker Team, 2017), which was the observation data used in CarbonTracker 2016 (Peters et al., 2007, with updates documented at http://carbon-tracker.noaa.gov). It is a subset of the Observation Package (ObsPack) Data Product (ObsPack, 2016), and contains a collection of discrete and quasi-continuous measurements at surface, tower

and ship sites contributed by national and universities laboratories around the world. In this study, in situ measurements from 78 sites provided by this product are used for inversion. Among these 78 sites, there are 56 flask sites, of which 52 sites are selected to evaluate the posterior $CO_2$ concentrations (selection criteria given in Section 4.1.1).

TCCON is a network of ground-based Fourier Transform Spectrometers that measure direct near-infrared solar absorption spectra. Column-averaged abundances of atmospheric constituents including $CO_2$, $CH_4$, $N_2O$, HF, CO, $H_2O$, and HDO are retrieved through these spectra. We use $XCO_2$ retrievals from 13 stations from TCCON GGG2014 dataset (Blumenstock et al., 2017; Deutscher et al., 2017; Griffith et al., 2017a, b; Kivi et al., 2017; Morino et al., 2017; Notholt et al., 2017a, b; Sherlock et al., 2017; Sussmann and Rettinger, 2017; Warneke et al., 2017; Wennberg et al., 2017a, b). The names of the 13 stations are Bialystok (Bial), Bremen (Brem), Orleans (Orle), Garmisch (Garm), Darwin (Darw), Izana (Izan), Ny Alesund (Ny_A), Lamont (Lamo), Lauder (Laud), Park Falls (Park), Sodankyla (Soda), Tsukuba (Tsuk), and Wollongong (Woll). The locations of in situ sites and 13 TCCON stations are shown in Figure 2.

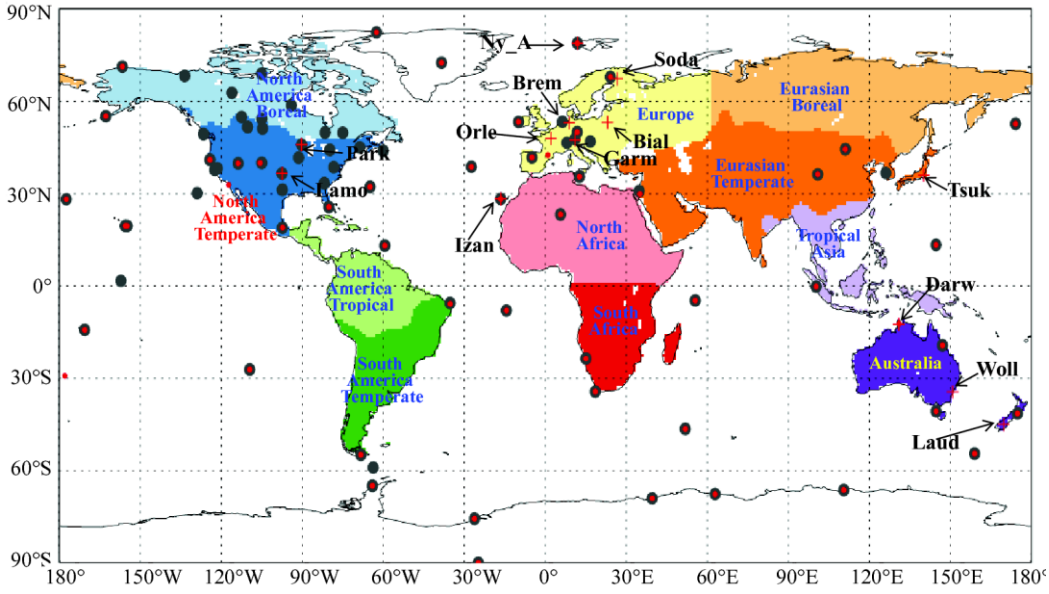


**Figure 2.** Distributions of the observation sites used in this study. Gray solid circles are surface sites used in the in situ inversion, red points and red cross marks are surface flask and TCCON sites used for evaluations, respectively, the shaded area shows the 11 TRANSCOM regions

## 2.3 GEOS-Chem 4DVAR assimilation framework

### 2.3.1 GEOS-Chem model

GEOS-Chem model (http://geos-chem.org) is a global three-dimensional chemistry transport model (CTM), which is driven by assimilated meteorological data from the Goddard Earth Observing System (GEOS) of the NASA Global Modeling and Assimilation Office (GMAO) (Rienecker et al., 2008). The original $CO_2$ simulation in the GEOS-Chem model was developed by Suntharalingam et al. (2004) and accounts for $CO_2$ fluxes from fossil fuel combustion and cement production, biomass burning, terrestrial ecosystem exchange, ocean exchange and biofuel burning. Nassar et al. (2010) updated the $CO_2$ simulation with improved inventories. In addition to the inventories in earlier version, the new $CO_2$ fluxes includes $CO_2$ emissions from international shipping, aviation (3D) and the chemical production of $CO_2$ from CO oxidation throughout the troposphere. In most other models, the oxidation of CO was treated as direct surface $CO_2$ emissions. The details of the $CO_2$ simulation and the $CO_2$ sinks/sources inventories could be found in Nassar et al. (2010). The version of GEOS-Chem model used in this study is v8-02-01.

### 2.3.2 GEOS-Chem adjoint model

An adjoint model is used to calculate the gradient of a response function of one model scalar (or cost function) with respect to a set of model parameters. The adjoint of the GEOS-Chem model was first developed for inverse modeling of aerosol (or their precursors) and gas emissions (Henze et al., 2007). It has been implemented to constrain sources of species such as CO, $CH_4$, and $O_3$ with satellite observations (Kopacz et al., 2009, 2010; Jiang et al., 2011; Wecht et al., 2012; Parrington et al., 2012). Several studies have successfully used this adjoint model to constraint carbon sources and sinks with surface flask measurements of $CO_2$ mixing ratio and space-based $XCO_2$ retrievals (Deng et al., 2014; Liu et al., 2014; Deng et al., 2016; Liu et al., 2017).

### 2.3.3 Inversion method

In the GEOS-Chem inverse modeling framework, the 4D-Var data assimilation technique is

employed for combining observations and simulations to seek a best optimal estimation of the state of a system. The scaling factors are applied to the carbon flux components to be optimized monthly in each model grid point. This approach seeks the scaling factors of the carbon flux that minimize the cost function, J, given by:

$$J(\mathrm{c}) = \frac{1}{2}\sum_{i=1}^{N}\left(XCO_{2,i}^{m} - XCO_{2,i}^{obs}\right)S_{obs,i}^{-1}\left(XCO_{2,i}^{m} - XCO_{2,i}^{obs}\right) + \left(\frac{1}{2}(c - c_a)S_c^{-1}(c - c_a)\right) \quad (1)$$

where N is total number of satellite $XCO_2$ observations; $XCO_2^m$ and $XCO_2^{obs}$ are modeled and observed total column averaged dry air mole faction of $CO_2$ respectively; $c_a$ is the prior scaling factor of the carbon flux, which is typically set as unity; $S_{obs}$ is the model-data mismatch error covariance matrix; $S_c$ is the scaling factor error covariance matrix. The gradients of the cost function with respect to scaling factors calculated with the adjoint model are supplied to an optimization routine (the L-BFGS-B optimization routine; Byrd et al., 1995; Zhu et al., 1994), and the minimum of the cost function is sought iteratively.

For the modeled $CO_2$ column to be comparable with the satellite $XCO_2$ retrievals, the modeled $CO_2$ concentration profile should be first mapped into the satellite retrieval levels and then convoluted with retrieval averaging kernels. The modeled $XCO_2$ is computed by:

$$XCO_2^m = XCO_2^a + \sum_j h_j a_j (A(x) - y_{a,j}) \quad (2)$$

where *j* denotes retrieval level, *x* is the modeled $CO_2$ profile; ***A(x)*** is a mapping matrix; $XCO_2^a$ is prior $XCO_2$, $h_j$ is pressure weighting function, $a_j$ is the satellite column averaging kernel and $y_a$ is the prior $CO_2$ profile for retrieval. These last four quantities are provided from ACOS Version 7.3 Level 2 Lite products.

## 3. Inversion settings

In this study, the GEOS-Chem model was run in a horizontal resolution of 2°×2.5° for 47 verti-

cal layers. Three inversions, using GOSAT data, OCO-2 data, and in situ measurements, are conducted from Oct 1, 2014 to December 31, 2015, respectively. Poor-man inversion, based on global atmospheric $CO_2$ trend and using poor-man's method (Chevallier et al, 2009, 2010), is also conducted. The posterior dry air mole fraction of $CO_2$ on Oct 1, 2014 from CT2016 product is taken as the initial concentration. The first three months are taken as the spin-up period. The prior carbon fluxes used in this study include fossil fuel $CO_2$ emissions, biomass burning $CO_2$ emissions, terrestrial ecosystem carbon exchange and $CO_2$ flux exchange over the sea surface. Fossil fuel emissions are obtained from CT2016, which is an average of Carbon Dioxide Information Analysis Center (CDIAC) product (Andres et al., 2011) and Open-source Data Inventory of Anthropogenic $CO_2$ (ODIAC) emission product (Oda and Maksyutov, 2011). The biomass burning $CO_2$ emissions are also taken from CT2016, which are the average of the Global Fire Emissions Database version 4.1 (GFEDv4) (van der Werf et al., 2010; Giglio et al., 2013) and the Global Fire Emission Database from NASA Carbon Monitoring System (GFED_CMS). The 3-hourly terrestrial ecosystem carbon exchanges are from the Carnegie-Ames-Stanford Approach (CASA) model GFED4.1 simulation (Potter el al., 1993; van der Werf et al., 2010). $CO_2$ exchanges over the ocean surface are from the posterior air-sea $CO_2$ flux of CT2016. It is noted that the fossil fuel emissions and the biomass burning emissions in our inversions are kept intact. Both terrestrial ecosystem $CO_2$ exchanges and ocean flux are optimized in our inversions.

An efficient computational procedure for constructing non-diagonal scaling factor error covariance matrix which accounts for the spatial correlation of errors is implemented (Single et al., 2011). The construction is based on the assumption of exponential decay of error correlations. Other than forming covariance matrix explicitly, multiple-dimensional correlations are represented by tensor products of one-dimensional correlation matrices along longitude and latitudinal directions. For the two inversions, the scale lengths assigned along longitudinal and latitudinal directions are 500 km

and 400 km for terrestrial ecosystem exchange and 1000 km and 800 km for ocean exchange, respectively. No correlations between different types of fluxes are assumed. The temporal correlations are also neglected. Global annual uncertainty of 100% and 40% are assigned for terrestrial ecosystem and ocean $CO_2$ exchanges, respectively (Deng and Chen, 2011). Accordingly, the uncertainty of scaling factor for the prior land and ocean fluxes in each month at the grid cell level are assigned to 3 and 5, respectively.

### 3.1 Inversions using satellite $XCO_2$ retrievals

The observation error covariance matrix is constructed using the retrieval errors, which are provided along with the ACOS $XCO_2$ data. Observation errors are assumed to be uncorrelated at model grid level. To account for the correlated observation errors, as shown in section 2.1, the pixel level retrieval errors are filtered and averaged to the model grid level, and then inflated by a factor of 1.9 to ensure the chi-square testing of $\chi^2$ value to be close to 1 (Tarantola, 2004; Chevallier et al., 2007).

### 3.2 Inversion using in situ measurements

As described in section 2.2, surface $CO_2$ observations from 78 sites including flask samples and by quasi-continuous analyzer are adopted in this inversion. These data are selected from data collection of the ObsPackCT2016. The observation uncertainties of the 78 sites are also obtained from this product, which account for both the measurement and representative errors (Peters et al., 2007, with updates documented at http://carbontracker.noaa.gov). An examination for the differences between observations and forward model simulation was conducted (data not shown), and the results shows that observation uncertainties from CT2016 represents well with the model-data mismatch errors of GEOS-Chem model. In addition, we neglect correlations between observations and assume a diagonal observation error covariance matrix.

### 3.3 Poor-man inversion

A baseline inversion, which was introduced by Chevallier et al. (2009, 2010) as a poor-man's

method, is implemented to evaluate satellite retrievals and in situ measurements based inversions. Usually, the posteriori fluxes are evaluated by the improvement on the simulated $CO_2$ mixing ratios. Since the global $CO_2$ trend can be accurately estimated from marine sites, it is important to assess whether the inverted flux can capture more information than this trend. In this baseline inversion, the ocean flux is kept identical to the prior ones. The poor-man's inverted land flux $F_{pm}$ at location ($x$, $y$) and at time $t$ is defined as:

$$F_{pm}(x, y, t) = F_{prior}(x, y, t) + k \times \sigma(x, y, t) \quad (3)$$

where $F_{prior}$ is the prior flux, $\sigma$ is the uncertainty of the prior flux, $k$ is a coefficient, it can be solved directly from the formula (3) as

$$k = \left(\sum F_{pm}(x, y, t) - \sum F_{prior}(x, y, t)\right) / \sum \sigma(x, y, t) \quad (4)$$

where $\sum F_{pm}(x, y, t)$ equals the global total land flux, which can be calculated from the observed annual global $CO_2$ growth rate, global annual fossil fuel and biomass burning emissions, and ocean flux. In this study, the observed annual global $CO_2$ growth rate is from the Global Monitoring Division (GMD) of NOAA/Earth System Research Laboratory (ESRL) (Ed Dlugokencky and Pieter Tans, NOAA/ESRL, www.esrl.noaa.gov/gmd/ccgg/trends/). The annual global $CO_2$ growth rate is 2.96 ppm in 2015, which is converted to 6.28 PgC $yr^{-1}$ for the poor-man's global total by multiplying by a factor of 2.123 PgC $ppm^{-1}$.

## 4. Results and Discussions

### 4.1 Evaluation for the inversion results

#### 4.1.1 Flask observations

As shown in section 2.2, Flask observations from 52 sites are used to evaluate the inversion results. Actually, there are much more flask observations in the dataset. When there are more than one flask dataset for one site, we give priority to that from NOAA/ESL or that with more consistent records. There are 56 sites with available flask observations for evaluation. In addition, during the

evaluations, we find that GEOS-Chem model is unable to capture the variations of $CO_2$ mixing ratios at HPB, HUN, SGP and TAP sites, where the standard deviations of the deviations between the observed and modeled mixing ratio are larger than 5 ppm. Therefore, we exclude these four sites and use the rest 52 flask sites (shown in Figure 2) to evaluate the posterior mixing ratios. The GEOS-Chem model is driven with the prior flux and the four posterior fluxes to obtain the prior and posterior $CO_2$ mixing ratios. The simulated $CO_2$ mixing ratios are sampled at each observation site and within half an hour of observation time.

Table 1 shows a summary of comparisons of the simulated $CO_2$ mixing ratios against the flask measurements. The mean difference between the prior $CO_2$ mixing ratio and the flask measurements is 0.93 ppm, with a standard deviation of 2.3 ppm. All four inversions show improvement in posterior concentrations with reductions of biases. Not surprisingly, in situ inversion, using surface observations which include all the flask measurements used for evaluation, shows the best improvement in posterior $CO_2$ mixing ratio with the largest reduction of bias and standard deviation. GOSAT inversion achieves almost the same reductions of standard deviation as in situ inversion. OCO-2 inversion gives larger bias and standard deviation than in situ and GOSAT inversions. Poor-man inversion effectively reduces the bias but with little improvement in the reduction of standard deviations.

Figure 3 shows the biases at each observation site in different latitudes. It could be found that the biases between the simulations and the observations in the northern hemisphere are significantly larger than those in southern hemisphere since the carbon flux distribution of the northern hemisphere is more complex than that of the southern hemisphere. When the prior flux is used, almost all sites in the northern hemisphere have significant positive deviations, with an average of 1.7 ppm, while in the southern hemisphere, the deviations are very small, with an average bias of only -0.08 ppm; when using the posteriori flux from OCO-2 inversion, the deviations in most northern hemisphere sites are slightly reduced, with an average deviation of 0.85 ppm, while in the southern hemisphere, at most sites, the biases increase by variable amounts, with a mean of -0.13 ppm; when using the posterior

flux from GOSAT inversion, the deviations are significantly reduced to 0.04 ppm in the northern hemisphere but further increased to -0.55 ppm in the southern hemisphere. In situ inversion shows similar improvement in Northern Hemisphere as GOSAT inversion does, but also with little improvement in Southern Hemisphere. Though poor-man inversion effectively reduces the global bias, it shows largest negative biases in Southern Hemisphere and moderate positive biases (close to OCO-2 inversions) in Northern Hemisphere, indicating that the improvements of poor-man inversion for posterior concentrations are very limited. These suggest that GOSAT and in situ inversions can effectively improve the carbon fluxes estimate in the northern hemisphere, but overestimate the land sinks in the southern hemisphere.

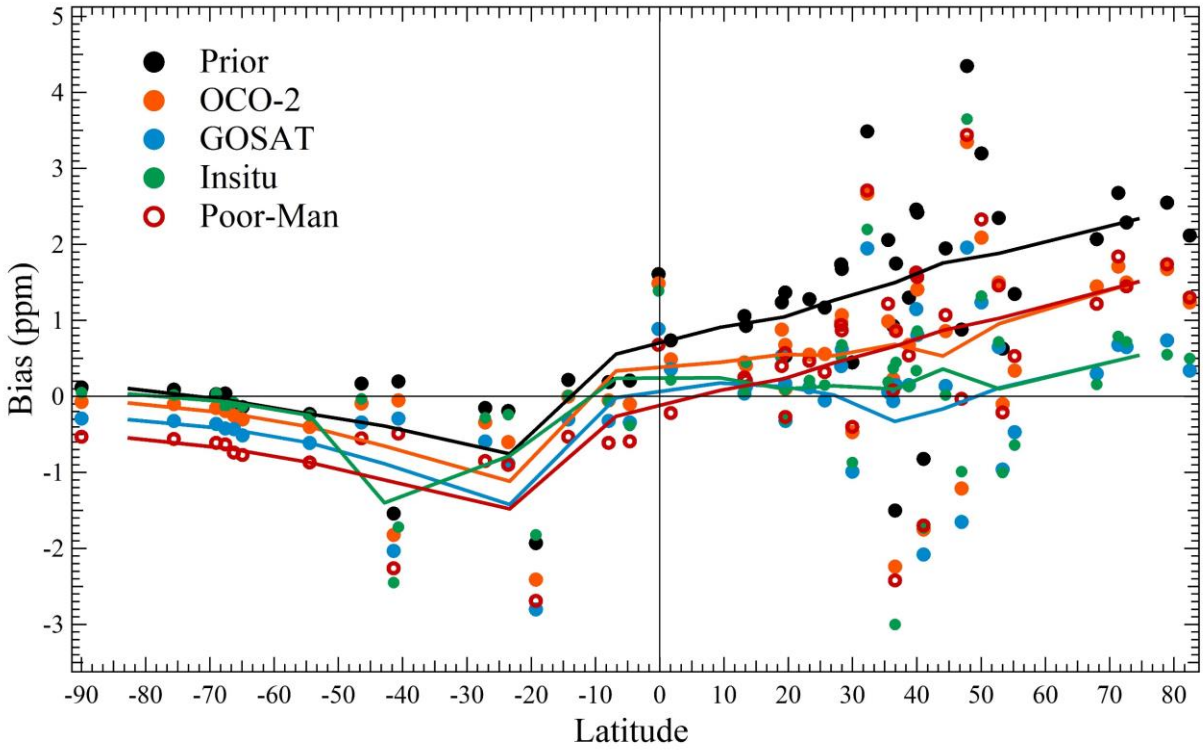


**Figure 3**. Biases of the simulated $CO_2$ mixing ratios against the flask measurements in different latitudes (positive/negative biases represent modeled concentration being greater/less than the observed, the different color lines are the smooth of the corresponding marks)

4.1.2 TCCON observations

We also use data from 13 TCCON sites (Figure 2) to evaluate our inversion results. The simu-

316 lated $CO_2$ concentrations at 47 vertical levels are mapped onto 71 TCCON levels. Following the ap-
317 proach of Wunch et al. (2011), using prior profiles and the averaging kernel from the TCCON da-
318 taset, we calculated the modeled $XCO_2$ values at 13 TCCON sites. It should be noted that the com-
319 parisons of posterior $XCO_2$ from GOSAT and OCO-2 inversions with TCCON data are not fully
320 independent since the TCCON data were used in the bias-correction scheme of both GOSAT and
321 OCO-2 products (Wunch et al., 2011). Table 1 also shows the comparison of modeled $XCO_2$ with
322 TCCON observations. The mean difference between prior $XCO_2$ and TCCON retrievals is 1.16
323 ppm, with a standard deviation of 1.3 ppm. GOSAT inversion performs the best with the largest re-
324 ductions of bias and standard deviation. Though OCO-2 inversion shows improvement in the reduc-
325 tion of standard deviation, it gives a relatively large bias for posterior $XCO_2$. In situ inversion has
326 the same reduction of standard deviation as GOSAT inversion. Poor-man inversion reduces the bias
327 to 0.49 ppm and gives slight improvement in reducing standard deviation of posterior $XCO_2$.

328 Figure 4 shows the bias at each TCCON site. Obviously, the biases at all TCCON sites are pos-
329 itive when using the prior fluxes, ranging between 0.3 and 2.6 ppm. The biases at the sites in the
330 northern temperate and boreal areas are all above 1.5 ppm except for the Lamo site. GOSAT and in
331 situ inversions significantly reduce the biases at most sites. However, in Northern Hemisphere, the
332 biases at those sites remain relatively large. Since GOSAT and in situ inversions show evident im-
333 provement at flask sites in Northern Hemisphere, the remaining large biases at TCCON sites may
334 be also related to the biases of TCCON retrievals (Wunch et al, 2010; Messerschmidt et al, 2011).
335 OCO-2 and poor-man inversions show slight improvement in the reduction of biases at most sites
336 and rather large biases still remain.

337 Overall, it also could be found from Table 1 that only in situ inversion beats the poor-man in-
338 version on all 4 statistics, followed by GOSAT inversion, which beats the poor-man on 3 statistics,
339 indicating that in situ measurements have the best performance among all inversions, and GOSAT
340 retrieval have similar performance as in situ data.

**Table 1**. Statistics of the model-data mismatch errors at the 52 surface flask sites and the 13 TCCON sites (ppm)

| | Flask | | TCCON | |
|---|---|---|---|---|
| | Bias | Stdev | Bias | Stdev |
| Prior | 0.93 | 2.30 | 1.16 | 1.30 |
| OCO-2 | 0.33 | 2.15 | 0.80 | 1.08 |
| GOSAT | -0.19 | 2.05 | 0.22 | 1.04 |
| In situ | -0.03 | 2.04 | 0.38 | 1.04 |
| Poor-man | 0.14 | 2.28 | 0.49 | 1.25 |

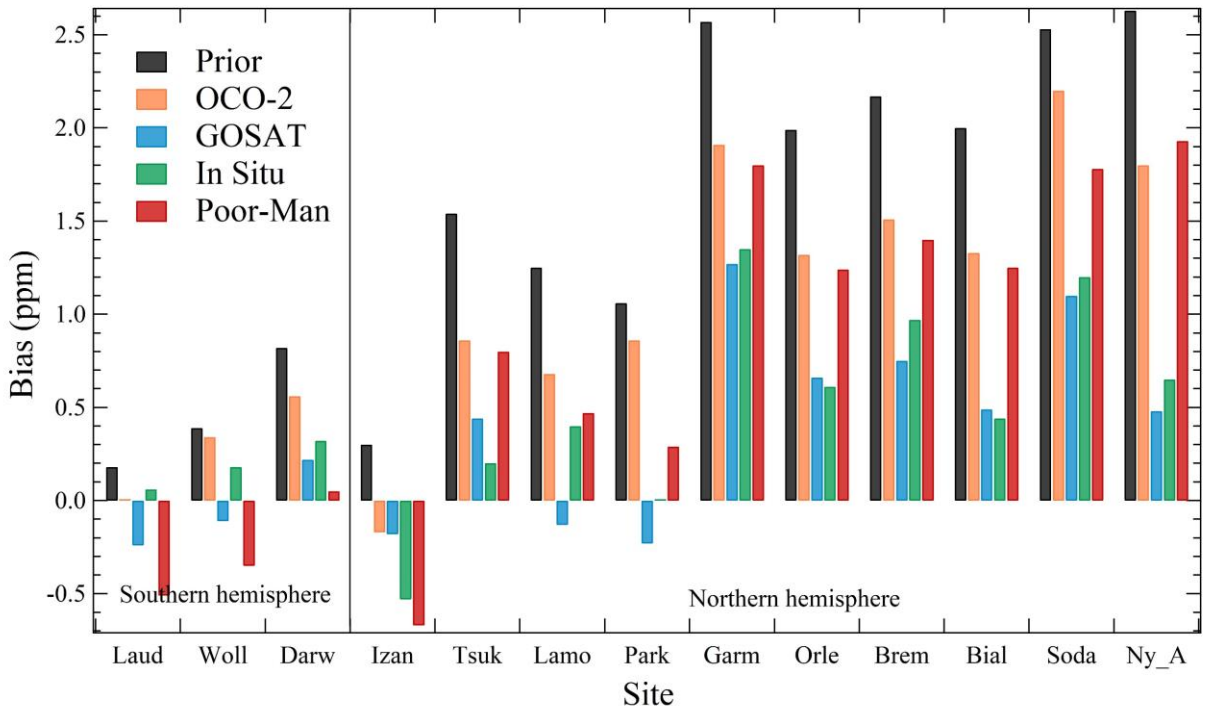


**Figure 4**. The biases between the modeled and observed $XCO_2$ at the 13 TCCON sites

## 4.2 Global carbon budget

Table 2 presents the global carbon budgets in 2015 from four inversions. The global land sinks inferred by GOSAT and OCO-2 $XCO_2$ retrievals are -3.48 and -2.94 PgC $yr^{-1}$, respectively, which

are both larger than the prior value, and lower than the estimate from the in situ inversion. The differences of ocean fluxes among a priori and two inversions are small since we don't assimilate $XCO_2$ data over ocean. The global net flux from the poor-man inversion is inferred from the global annual $CO_2$ growth rate, which represents relatively accurately the net carbon flux added into atmosphere. It could be found that the global net flux from GOSAT inversion is the closest to the poor-man inversion estimate, while that from OCO-2 inversion is higher and the in situ inversion estimate is lower than the poor-man estimate, indicating that GOSAT inversion has the best estimates for the land and ocean carbon uptakes, while those from in situ inversion are overestimated, and those from OCO-2 inversion might be underestimated.

**Table 2**. Global carbon budgets estimated by the OCO-2 and GOSAT inversions in this study as well as those from the prior fluxes, in situ and poor-man inversions (PgC $yr^{-1}$)

| | Prior | OCO-2 | GOSAT | In situ | Poor-man |
|---|---|---|---|---|---|
| Fossil fuel and industry | 9.84 | 9.84 | 9.84 | 9.84 | 9.84 |
| Biomass burning emissions | 2.20 | 2.20 | 2.20 | 2.20 | 2.20 |
| Land sink | -2.50 | -2.94 | -3.48 | -3.63 | -3.35 |
| Ocean sink | -2.41 | -2.44 | -2.45 | -2.41 | -2.41 |
| Global net flux | 7.13 | 6.66 | 6.11 | 6.00 | 6.28 |

### 4.3 Regional carbon flux

Figure 5 shows the distributions of annual land and ocean carbon fluxes (excluding fossil fuel and biomass burning carbon emissions, same thereafter) of the prior and the estimates using GOSAT and OCO-2 data. It could be found that compared with the prior fluxes, the carbon sinks in Central America, south and northeast China, east and central Europe, south Russia and east Brazil are obviously increased in GOSAT inversion. Except for east Brazil, the land sinks in those areas in OCO-2 inversion are also increased, but much weaker than those in GOSAT inversion, and in east Brazil, it turns to a significant carbon source. In contrast, in east and central Canada, north Russia, north Europe, west Indo-China Peninsula, north Democratic Republic of the Congo and west Brazil, their

carbon sources are significantly increased in both GOSAT and OCO-2 inversions. In east and central Canada, north Europe and west Brazil, there are much stronger carbon sources in OCO-2 inversion.

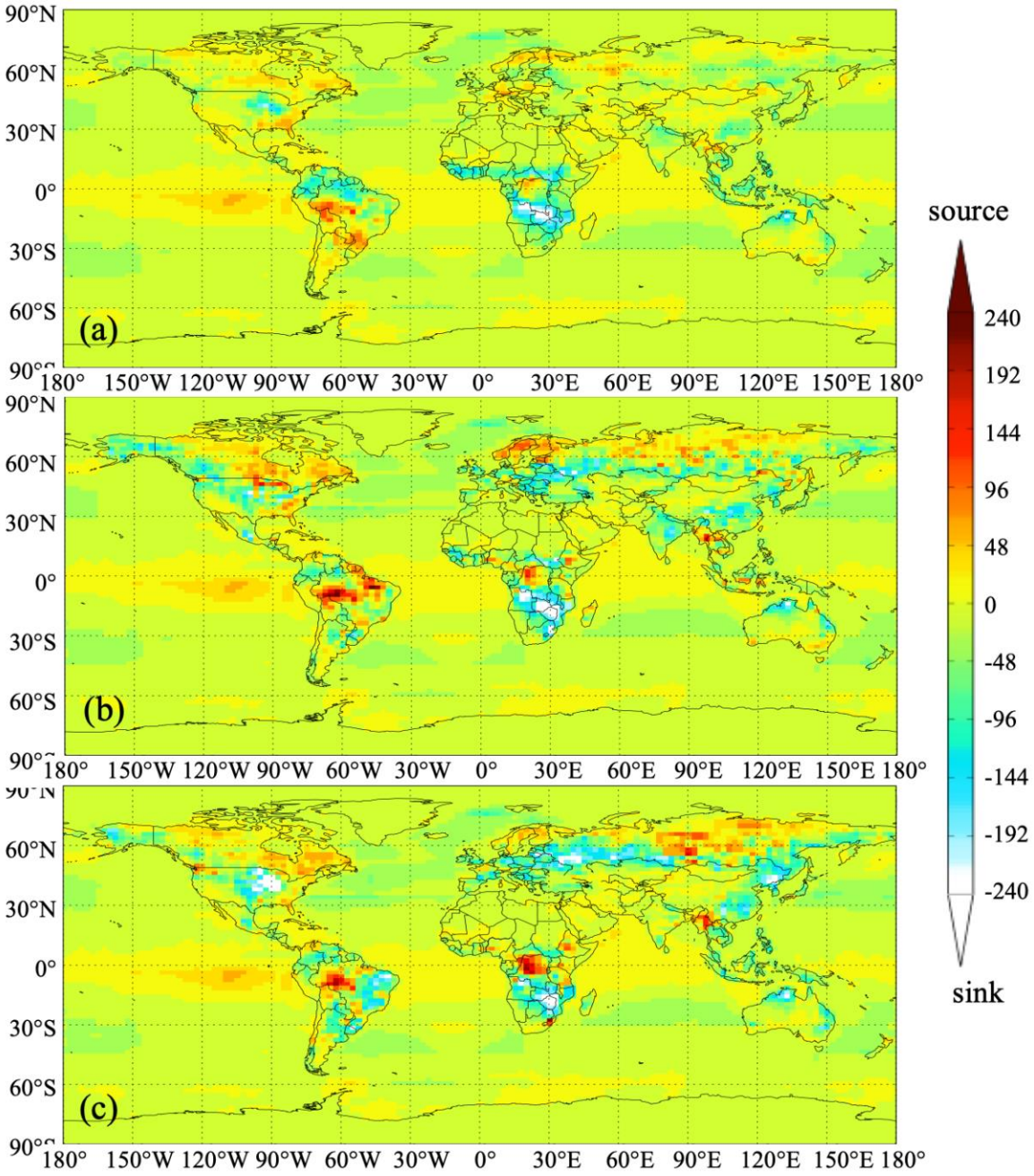


**Figure 5**. Distributions of annual land and ocean carbon fluxes a) prior flux and posterior fluxes based on (b) OCO-2 and (c) GOSAT data (gC $m^{-2}yr^{-1}$)

To better investigate the differences between GOSAT and OCO-2 inversions as well as their differences with two other inversions, we aggregate the prior and inferred land fluxes into 11 TRANS-COM land regions (Gurney et al., 2002) as shown in Figure 2. Figure 6 shows aggregated annual land

surface fluxes from the prior and inversions for the 11 land regions. Clearly, in most regions, the land sinks inverted based on GOSAT data are stronger than those inferred from OCO-2 data, especially in the Temperate and Tropical Lands. For example, in South America Temperate, the estimated land sink based on GOSAT data is about 4 times as large as the OCO-2 inversions; in North America Temperate and Tropical Asia, the carbon sinks of GOSAT experiment is about twice that of the OCO-2 inversions; and in South America Tropical, the OCO-2 inversion result is a carbon source of 0.19 PgC $yr^{-1}$, while GOSAT inversion gives a weak sink of -0.05 Pg C $yr^{-1}$. The total sinks of the Temperate/Tropical Lands optimized using GOSAT and OCO-2 $XCO_2$ retrievals are -2.95/-0.36 and -2.59/-0.20 Pg C $yr^{-1}$, respectively (Table 3). In Northern Boreal Land, the total carbon sinks inverted with GOSAT and OCO-2 data are comparable. However, the two $XCO_2$ data have opposite performances in two northern boreal regions, namely in Eurasian Boreal, the inverted land sink with GOSAT is stronger than that with OCO-2; while in North America Boreal, it is the opposite.

For different continents (Table 3), in Asia and Australia, their carbon sinks inverted from GOSAT and OCO-2 data are comparable. In North America, South America and Europe, the land sinks in GOSAT inversion are much stronger than those in OCO-2 inversion. Especially in South America, the GOSAT inversion result is a strong carbon sink (-0.51 Pg C $yr^{-1}$), while in OCO-2 inversion, it is a weak carbon source (0.06 Pg C $yr^{-1}$). Conversely, in Africa, the land sink estimated with GOSAT data is much weaker than those from OCO-2 data, the former (-0.59 Pg C $yr^{-1}$) being only about the half of the latter (-1.13 Pg C $yr^{-1}$).

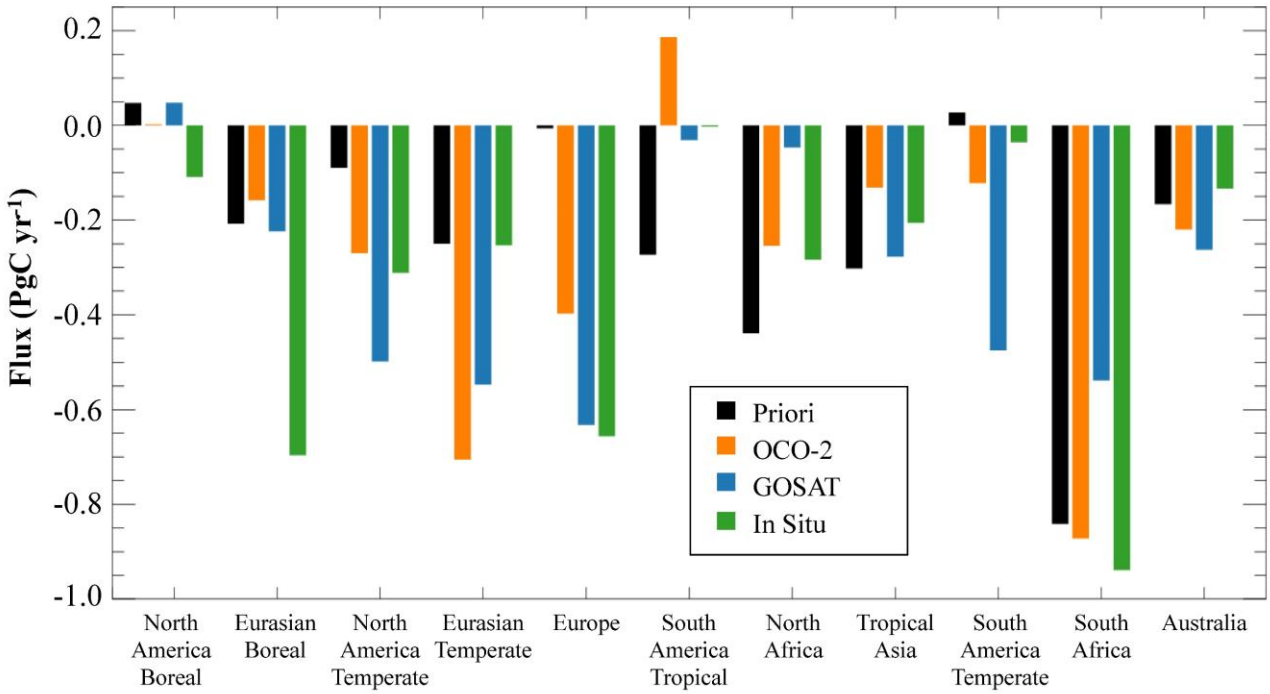


400

401 **Figure 6**. Aggregated annual land fluxes of the 11 TRANSCOM land regions

402 **Table 3**. The prior and posterior fluxes in six continents and boreal, temperate and tropical lands (PgC
403 $yr^{-1}$)

| Regions | Prior | OCO-2 | GOSAT | In situ |
|---|---|---|---|---|
| North America | -0.04 | -0.27 | -0.45 | -0.42 |
| South America | -0.25 | 0.06 | -0.51 | -0.04 |
| Europe | -0.01 | -0.40 | -0.63 | -0.66 |
| Asia | -0.76 | -0.99 | -1.05 | -1.16 |
| Africa | -1.28 | -1.13 | -0.58 | -1.22 |
| Australia | -0.17 | -0.22 | -0.26 | -0.13 |
| Northern Boreal Land | -0.16 | -0.16 | -0.18 | -0.81 |
| Northern Temperate Land | -0.35 | -1.37 | -1.68 | -1.22 |
| Tropical Land | -1.01 | -0.20 | -0.36 | -0.49 |
| Southern Temperate Land | -0.98 | -1.21 | -1.28 | -1.11 |

404

405 Compared with the in situ inversion, in the boreal regions, the land sinks estimated from GOSAT
406 and OCO-2 inversions are much weaker than those from in situ inversion, especially in the Eurasian
407 Boreal, the land sink estimated by in situ inversion is more than two times larger than the estimates

of GOSAT and OCO-2 inversions. In the tropical land, the total land sinks inferred from both GOSAT and OCO-2 inversions are weaker than those from the in situ inversion, but in different regions, the situations are different. In the Temperate lands, except for Europe and south Africa, the land sinks from GOSAT and OCO-2 inversions are much stronger than those from the in situ inversion. For example, in South America Temperate, GOSAT inversion shows a strong carbon sink, while in situ inversion shows a weak source. For different continents, in North America, Asia, Europe, the carbon sinks inferred from GOSAT inversion are comparable to those from in situ inversion, while in South America and Africa, the carbon sinks inferred from OCO-2 inversion are much closer to the in situ inversion.

Compared with the prior fluxes, the inferred land fluxes in Northern Temperate regions have the largest changes, followed by those in Tropical regions and Southern Temperate lands, while in boreal regions, the changes are the smallest. As shown in Table 4, for different TRANSCOM regions and different $XCO_2$ used, the changes of carbon fluxes have large differences. Since the same setup used in these two inversions and the same algorithm adopted for retrieving $XCO_2$ from GOSAT and OCO-2 measurements, the different impacts of $XCO_2$ data on land sinks may be related to the spatial coverage and the amount of data in these two $XCO_2$ datasets. As shown in Figure 1, in different latitude zones, the spatial coverage and the data amount of GOSAT and OCO-2 have large differences. Statistics show that the amount of data is largest in northern temperate land, followed by southern temperate land and tropical land, and least in northern boreal regions, corresponding to the magnitude of changes of carbon fluxes in these zones. For one specific zone, the different impacts of these two $XCO_2$ datasets may be also related to their data amount. For example, in northern temperate land, GOSAT has more $XCO_2$ data than OCO-2. Accordingly, the change of carbon flux caused by GOSAT is larger than that caused by OCO-2. Conversely, in Tropical Land, OCO-2 has more data than GOSAT, and as shown before it has more significant impact on the land sink. This relationship could also be found in each TRANSCOM region. Figure 5 gives a relationship between the $XCO_2$ data amount

ratios of GOSAT to OCO-2 and the land sinks absolute change ratios caused by GOSAT to OCO-2 for 11 TRANSCOM land regions. Obviously, except for North and South Africa, there is a significant linear correlation ($R$=0.95) between these two ratios, suggesting that with more $XCO_2$ data, the more carbon flux relative to the prior flux is changed. In North Africa, we find that OCO-2 has better spatial coverage and more data than GOSAT, as shown in Figure 1. Although the differences mainly occur in the Sahara where the carbon flux is very weak, but near the equatorial region where the carbon flux is large, OCO-2 still has more data than GOSAT. In southern Africa, both $XCO_2$ have good spatial coverage, the amount of GOSAT data is about 1.5 times that of OCO-2, but the changes in the carbon flux caused by GOSAT is about 10 times that of OCO-2. The large ratio of carbon change is mainly due to the relatively small carbon change from OCO-2 inversion.

**Table 4**. Differences between the inferred and the prior carbon fluxes, the data amount of $XCO_2$ and the deviations between the modeled with prior flux and satellite retrieved $XCO_2$ in different regions

| Region | Flux changed (Pg C $yr^{-1}$)* | | $XCO_2$ data amount | | Deviations (ppm)** | |
|---|---|---|---|---|---|---|
| | OCO-2 | GOSAT | OCO-2 | GOSAT | OCO-2 | GOSAT |
| North America Boreal | -0.05 | 0 | 1143 | 639 | 0.6 | 1.41 |
| North America Temperate | -0.18 | -0.41 | 2390 | 3163 | 0.52 | 0.93 |
| South America Tropical | 0.46 | 0.24 | 800 | 421 | -0.89 | 0.43 |
| South America Temperate | -0.15 | -0.5 | 1711 | 3500 | 0.02 | 0.54 |
| North Africa | 0.19 | 0.39 | 3208 | 674 | 0.12 | -0.19 |
| South Africa | -0.03 | 0.3 | 2057 | 3060 | 0.17 | 0.33 |
| Eurasian Boreal | 0.05 | -0.02 | 1714 | 1339 | 0.47 | 1.5 |
| Eurasian Temperate | -0.46 | -0.3 | 5323 | 4782 | 0.46 | 0.82 |
| Tropical Asia | 0.17 | 0.03 | 726 | 550 | -0.43 | 0.34 |
| Australia | -0.05 | -0.1 | 2011 | 3110 | 0.18 | 0.67 |
| Europe | -0.39 | -0.63 | 1604 | 2106 | 0.28 | 1.35 |
| Global land | -0.44 | -0.98 | 22687 | 23344 | 0.22 | 0.79 |
| Northern Boreal Land | 0.005 | -0.02 | 2857 | 1978 | 0.52 | 1.47 |
| Northern Temperate Land | -1.03 | -1.33 | 9317 | 10051 | 0.45 | 0.96 |
| Tropical Land | 0.82 | 0.66 | 4734 | 1645 | -0.08 | 0.13 |
| Southern Temperate Land | -0.23 | -0.3 | 5779 | 9670 | 0.11 | 0.6 |

* Differences between posterior and prior flux

** Deviations between the modeled $XCO_2$ with prior flux and satellite retrieved $XCO_2$

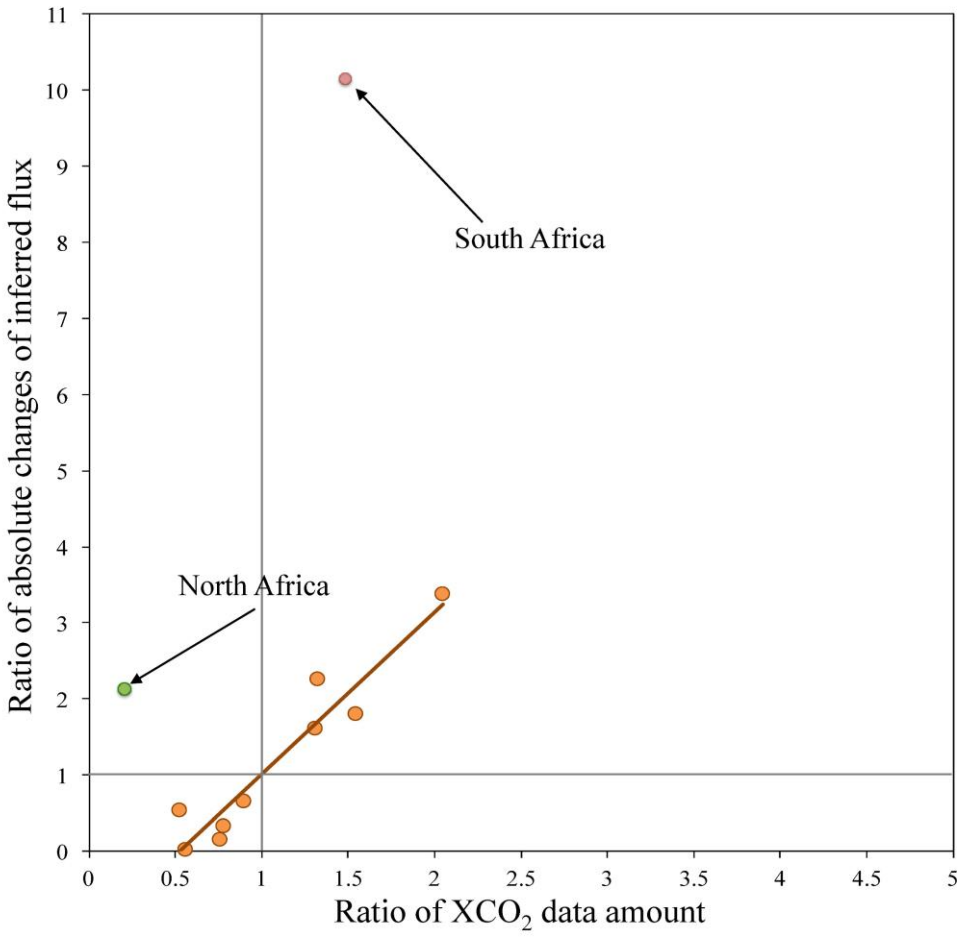


**Figure 7.** Scatter plot for the ratio of GOSAT to OCO-2 $XCO_2$ data amount versus the ratio of absolute changes of the land sinks caused by GOSAT to OCO-2 in the 11 TRANSCOM land regions

In addition to the data amount, the mismatches between the simulated $CO_2$ concentrations using prior fluxes and the satellite retrievals could be used to examine the performances of OCO-2 and GOSAT retrievals in different regions. Usually, a large model-data mismatch will impose strong constraint on the prior flux in inversions. Therefore, we compare the mismatches in OCO-2 and GOSAT inversions. The results are grouped global land and into the 11 TRANSCOM land regions, as shown in Table 4. The global land mean difference between modeled $XCO_2$ and the OCO-2 and GOSAT retrievals are 0.22 and 0.79 ppm, respectively, indicating that the GOSAT retrieval would have stronger constraint on the prior fluxes. In most TRANSCOM regions except North Africa, the mismatches in GOSAT inversion are positive and larger than those of OCO-2 inversion. In Tropic Asia and South America Tropic, the sizable negative mismatches in OCO-2 inversion could account

for a weak inverted carbon sink and an inverted carbon source in these two regions, while in North Africa, the negative mismatch in GOSAT inversion may explain why a rather weak sink is inverted for this region. The difference of mismatch between OCO-2 and GOSAT inversions exhibits rather large spread, ranging from 0.16 to 1.33 pm, indicating the biases of two satellite $XCO_2$ retrievals differ greatly.

**Table 5**. Statistics of the OCO-2 and GOSAT retrievals uncertainties against the TCCON retrievals

| | OCO-2 | | | GOSAT | | |
|---|---|---|---|---|---|---|
| | Bias (ppm) | Stdev (ppm) | N. of Obs. | Bias (ppm) | Stdev (ppm) | N. of Obs. |
| Bial | 0.91 | 1.47 | 21 | 0.06 | 1.35 | 29 |
| Darw | 0.75 | 0.85 | 43 | -0.41 | 1.62 | 44 |
| Garm | -0.10 | 2.97 | 14 | 0.73 | 2.02 | 35 |
| Lamo | 0.04 | 1.09 | 56 | -0.91 | 1.39 | 82 |
| Laud | 0.59 | 1.38 | 18 | -0.79 | 1.70 | 30 |
| Orle | 1.49 | 1.18 | 24 | -0.51 | 1.38 | 39 |
| Park | 0.50 | 1.26 | 29 | -0.58 | 1.52 | 38 |
| Soda | 1.91 | 1.89 | 7 | -0.54 | 2.58 | 9 |
| Tsuk | 0.93 | 1.95 | 16 | -0.47 | 1.11 | 38 |
| Woll | 0.34 | 1.07 | 27 | -0.36 | 1.56 | 45 |
| All | 0.60 | 1.45 | 255 | -0.42 | 1.59 | 389 |

Moreover, the uncertainties of OCO-2 and GOSAT retrievals may be another reason for the different performances in these two inversion experiments. We use TCCON retrieval to evaluate the uncertainties of OCO-2 and GOSAT $XCO_2$ retrievals. For satellite retrievals falling in the model grid box where TCCON sites are located, the closest TCCON retrievals in time or within two hours of satellite overpass time are chosen for comparison. We follow the procedures in Appendix A of Wunch et al. (2011) to do both prior profile and averaging kernel corrections. Table 5 shows the biases and standard deviations grouped globally and at 10 TCCON sites where both OCO-2 and GOSAT retrievals are available for comparison. The locations of these 10 sites are shown in Figure 2. At most sites except Garm, OCO-2 retrievals have positive biases, while GOSAT retrievals tend to have negative bias except at Bial and Garm sites. It also could be found that the spread of GOSAT

data biases are small, falling in the range of -0.36 to -0.58 ppm at most sites, while the spread of OCO-2 data biases is relatively large, with biases greater than 0.7 ppm at more than half of sites, and in the range of 0.34 to 0.59 ppm only at 3 sites. Overall, GOSAT retrievals (-0.46 ppm) have lower bias than OCO-2 retrievals (0.6 ppm) and the difference between two retrievals is relatively large. It should be noted that due to the limited number of collocated satellite retrievals, the real bias difference might be below 1 ppm. As shown in Table 4, the difference of overall mismatches between GOSAT and OCO-2 data is 0.57 ppm. These indicate that although both OCO-2 and GOSAT products were bias-corrected using TCCON retrievals, the uncertainties of OCO-2 and GOSAT retrievals are still very large, especially for OCO-2 retrieval, resulting in the degraded performance of OCO-2 retrieval, which also suggest that the bias-correction scheme implemented may need to be improved.

## 5. Summary and Conclusions

In this study, we use both GOSAT and OCO-2 $XCO_2$ retrievals to constrain terrestrial ecosystem carbon fluxes from Oct 1, 2014 to Dec 31, 2015, using the GEOS-Chem 4D-Var data assimilation system. In addition, one inversion using in situ measurements and another inversion as a baseline, are also conducted. The posterior carbon fluxes estimated from these four inversions at both global and regional scales during Jan 1 to Dec 31, 2015 are shown and discussed. We evaluate the posterior carbon fluxes by comparing the posterior $CO_2$ mixing ratios against observations from 52 surface flask sites and 13 TCCON sites.

Globally, the terrestrial ecosystem carbon sink (excluding biomass burning emissions) estimated from GOSAT data is stronger than that inferred from OCO-2 data and weaker than that from in situ inversion, but closest to the poor-man inversion estimate. Regionally, in most regions, the land sinks inferred from GOSAT data are also stronger than those from OCO-2 data. Compared with the in situ inversion, GOSAT inversions have weaker sinks in Boreal and most Tropical lands, and much stronger ones in Temperate lands. Compared with the prior fluxes, the inferred land sinks are largely

503 increased in the temperate regions, and decreased in tropical regions. There are largest changes of the
504 prior fluxes in Northern Temperate regions, followed by Tropical and Southern Temperate regions,
505 and the weakest in boreal regions. The different impact of $XCO_2$ on the carbon fluxes in different
506 regions is mainly related to the spatial coverage and the amount of $XCO_2$ data. Generally, a larger
507 amount of $XCO_2$ data in a region is corresponding to a larger change in the inverted carbon flux in
508 the same region. The different biases of the two $XCO_2$ retrievals may also give rise to their different
509 inversion performances.

510 Evaluations of the inversions using $CO_2$ concentrations from flask measurements and TCCON
511 retrievals show that the simulated $CO_2$ concentrations with GOSAT posterior fluxes are much closer
512 to the observations than those with OCO-2 estimates. Compared with poor-man inversion, both GO-
513 SAT and in situ inversions show evident improvement with the similar reductions of both biases and
514 standard deviations of posterior concentrations, while OCO-2 inversion only displays slight improve-
515 ment over poor-man inversion. Generally, the posterior biases from GOSAT inversion are signifi-
516 cantly reduced in the northern hemisphere and are slightly increased in the southern hemisphere.
517 These suggest that GOSAT data can effectively improve the carbon fluxes estimate in the northern
518 hemisphere.

519 The GOSAT and OCO-2 $XCO_2$ retrievals used in this study are bias-corrected products. Never-
520 theless, there still exists apparent biases and the differences between these two satellites data are
521 obvious. The more reliable constraints on carbon flux call for the further reduction of satellite retrieval
522 errors. These indicate that we should interpret carbon flux inferred from the current satellites $XCO_2$
523 retrievals with great cautions in understanding global carbon cycle. It also should be noted that though
524 the OCO-2 $XCO_2$ retrievals of version b7.3 used in this study perform worse than GOSAT data and
525 in situ measurements in our inversions, one recent study has shown that the newer version of OCO-2
526 data has a much better performance in constraining carbon flux (Chevallier et al., 2019). With con-
527 stantly improved retrieval algorithm and bias-correction scheme, more robust estimate of carbon flux

from satellite $XCO_2$ retrievals could be achieved.

## Author contributions

FJ and HW designed the research, HW conducted inverse modeling, HW and FJ conducted data analysis and wrote the paper, JW, WJ and JC participated in the discussion of the results and provided input on the paper for revision before submission.

## Competing interests

The authors declare that they have no conflict of interest.

## Acknowledgements

This work is supported by the National Key R&D Program of China (Grant No: 2016YFA0600204), National Natural Science Foundation of China (Grant No: 41571452), and the Fundamental Research Funds for the Central Universities (Grant No: 090414380021). CarbonTracker CT2016 products are provided by NOAA ESRL, Boulder, Colorado, USA from the website at http://carbontracker.noaa.gov. The authors thank all contributing laboratories for providing in-situ $CO_2$ observations through ObsPack product obspack_co2_1_CARBONTRACKER_CT2016_2017-02-06, and TCCON PIs for making XCO2 measurements possible and available to the public. The authors are very grateful to Dr. Feng Deng at the University of Toronto for providing the module for in-situ data inversion, and for his valuable suggestions on running GEOS-Chem adjoint model. The authors would also like to thank two reviewers for their constructive comments which greatly improve the manuscript.

## References

Andres, R. J., Gregg, J. S., Losey, L., Marland, G. and Boden, T. A.: Monthly, global emissions of carbon dioxide from fossil fuel consumption. Tellus B, 63(3), 309–327, https://doi.org/10.1111/j.1600-0889.2011.00530.x, 2011.

Baker, D. F., Bösch, H., Doney, S. C., O'Brien, D., and Schimel, D. S.: Carbon source/sink information provided by column $CO_2$ measurements from the Orbiting Carbon Observatory, Atmos. Chem. Phys., 10, 4145–4165, https://doi.org/10.5194/acp-10- 4145-2010, 2010.

Basu, S., Guerlet, S., Butz, A., Houweling, S., Hasekamp, O., Aben, I., Krummel, P., Steele, P., Langenfelds, R., Torn, M., Biraud, S., Stephens, B., Andrews, A., and Worthy, D.: Global $CO_2$ fluxes estimated from GOSAT retrievals of total column $CO_2$, At- mos. Chem. Phys., 13, 8695–8717,

https://doi.org/10.5194/acp- 13-8695-2013, 2013.

Basu, S., Krol, M., Butz, A., Clerbaux, C., Sawa, Y., Machida, T., Matsueda, H., Frankenberg, C., Hasekamp, O. P., and Aben, I.: The seasonal variation of the $CO_2$ flux over Tropical Asia estimated from GOSAT, CONTRAIL, and IASI, Geophys. Res. Lett., 41, 1809–1815, https://doi.org/10.1002/2013GL059105, 2014.

Blumenstock, T., Hase, F., Schneider, M., García, O.E., and Sepúlveda, E.: TCCON data from Izana, Tenerife, Spain, Release GGG2014R1. TCCON data archive, hosted by CaltechDATA, California Institute of Technology, Pasadena, CA, U.S.A. https://doi.org/10.14291/tccon.ggg2014.izana01.R1, 2017.

Byrd, R. H., Nocedal, J. and Schnabel, R. B.: Representations of Quasi-Newton Matrices and their use in Limited Memory Methods. Math Program. 63(4), 129–156. https://doi.org/10.1007/BF01582063, 1994.

CarbonTracker Team; (2017): Simulated observations of atmospheric carbon dioxide from CarbonTracker release CT2016 (obspack_co2_1_CARBONTRACKER_CT2016_2017-02-06); NOAA Earth System Research Laboratory, Global Monitoring Division. http://dx.doi.org/10.15138/G3G599"

Chatterjee, A., Gierach, M. M., Sutton, A. J., Feely, R. A., Crisp, D., Eldering, A., Gunson, M. R., O'Dell, C. W., Stephens, B. B., and Schimel, D. S.: Influence of El Niño on atmospheric $CO_2$ over the tropical Pacific Ocean: Findings from NASA's OCO-2 mission, Science, 358, eaam5776, https://doi.org/10.1126/science.aam5776, 2017.

Chevallier, F., Breon, F.-M., and Rayner, P. J.: Contribution of the Orbiting Carbon Observatory to the estimation of $CO_2$ sources and sinks: Theoretical study in a variational data assimilation framework, J. Geophys. Res.-Atmos., 112, d09307, https://doi.org/10.1029/2006JD007375, 2007.

Chevallier, F., R. J. Engelen, C. Carouge, T. J. Conway, P. Peylin, C. Pickett-Heaps, M. Ramonet, P. J. Rayner, and I. Xueref-Remy (2009), AIRS-based versus flask-based estimation of carbon surface fluxes, J. Geophys. Res., 114, D20303, doi:10.1029/2009JD012311.

Chevallier, F., Ciais P., Conway T.J., Aalto T., Anderson B.E., Bousquet P., Brunke E.G., Ciattaglia L., Esaki Y., Fröhlich M., Gomez A., Gomez-Pelaez A.J., Haszpra L., Krummel P.B., Langenfelds R.L., Leuenberger M., Machida T., Maignan F., Matsueda H., Morguí J.A., Mukai H., Nakazawa T., Peylin P., Ramonet M., Rivier L., Sawa Y., Schmidt M., Steele L.P., Vay S.A., Vermeulen A.T., Wofsy S., and Worthy D.: $CO_2$ surface fluxes at grid point scale estimated from a global 21 year reanalysis of atmospheric measurements, J. Geophys. Res., 115, D21307, 2010.

Chevallier, F., Palmer, P. I., Feng, L., Boesch, H., O'Dell, C. W., and Bousquet, P.: Toward robust and consistent regional $CO_2$ flux estimates from in situ and spaceborne measurements of atmospheric $CO_2$, Geophys. Res. Lett., 41, 1065–1070, https://doi.org/10.1002/2013GL058772, 2014.

Chevallier, F., Remaud, M., O'Dell, C. W., Baker, D., Peylin, P., and Cozic, A.: Objective evaluation of surface- and satellite-driven $CO_2$ atmospheric inversions, Atmos. Chem. Phys. Discuss., https://doi.org/10.5194/acp-2019-213, in review, 2019.

Conway, T. J., Tans, P. P., Waterman, L. S., Thoning, K. W., Kitzis, D. R., Masarie, K. A., and Zhang, N.: Evidence for interannual variability of the carbon cycle from the National Oceanic and Atmospheric Administration/Climate Monitoring and Diagnostics Laboratory Global Air Sampling Network, J. Geophys. Res., 99, 22831–22855, https://doi.org/10.1029/94JD01951, 1994.

Crisp, D., Pollock, H. R., Rosenberg, R., Chapsky, L., Lee, R. A. M., Oyafuso, F. A., Frankenberg, C., O'Dell, C. W., Bruegge, C. J., Doran, G. B., Eldering, A., Fisher, B. M., Fu, D., Gunson, M. R., Mandrake, L., Osterman, G. B., Schwandner, F. M., Sun, K., Taylor, T. E., Wennberg, P. O., and Wunch, D.: The on-orbit performance of the Orbiting Carbon Observatory-2 (OCO-2) instrument and its radiometrically calibrated products, Atmos. Meas. Tech., 10, 59–81, https://doi.org/10.5194/amt-10-59-2017, 2017.

Deng, F. and Chen, J. M.: Recent global $CO_2$ flux inferred from atmospheric $CO_2$ observations and its regional analyses, Biogeo- sciences, 8, 3263–3281, https://doi.org/10.5194/bg-8-3263-2011, 2011.

Deng, F., Jones, D. B. A., Henze, D. K., Bousserez, N., Bowman, K. W., Fisher, J. B., Nassar, R., O'Dell, C., Wunch, D., Wennberg, P. O., Kort, E. A., Wofsy, S. C., Blumenstock, T., Deutscher, N. M., Griffith, D. W.

T., Hase, F., Heikkinen, P., Sherlock, V., Strong, K., Sussmann, R., and Warneke, T.: Inferring regional sources and sinks of atmospheric $CO_2$ from GOSAT $XCO_2$ data, Atmos. Chem. Phys., 14, 3703-3727, https://doi.org/10.5194/acp-14-3703-2014, 2014.

Deng, F., Jones, D. B. A., O'Dell, C. W., Nassar, R., and Parazoo, N. C.: Combining GOSAT $XCO_2$ observations over land and ocean to improve regional $CO_2$ flux estimates, J. Geophys. Res. Atmos., 121, 1896–1913, https://doi.org/10.1002/2015JD024157, 2016.

Deutscher, N., Notholt, J., Messerschmidt, J., Weinzierl, C., Warneke, T., Petri, C., Grupe, P., and Katrynski, K.: TCCON data from Bialystok, Poland, Release GGG2014R1. TCCON data archive, hosted by CaltechDATA, California Institute of Technology, Pasadena, CA, U.S.A. http://doi.org/10.14291/tccon.ggg2014.bialystok01.R1/1183984, 2017.

Eldering, A., Boland, S., Solish, B., Crisp, D., Kahn, P., and Gunson, M.: High precision atmospheric $CO_2$ measurements from space: The design and implementation of OCO-2, in: 2012 IEEE Aerospace Conference, 1–10, https://doi.org/10.1109/AERO.2012.6187176, 2012.

Eldering, A., O'Dell, C. W., Wennberg, P. O., Crisp, D., Gunson, M. R., Viatte, C., Avis, C., Braverman, A., Castano, R., Chang, A., Chapsky, L., Cheng, C., Connor, B., Dang, L., Doran, G., Fisher, B., Frankenberg, C., Fu, D., Granat, R., Hobbs, J., Lee, R. A. M., Mandrake, L., McDuffie, J., Miller, C. E., Myers, V., Natraj, V., O'Brien, D., Osterman, G. B., Oyafuso, F., Payne, V. H., Pol- lock, H. R., Polonsky, I., Roehl, C. M., Rosenberg, R., Schwand- ner, F., Smyth, M., Tang, V., Taylor, T. E., To, C., Wunch, D., and Yoshimizu, J.: The Orbiting Carbon Observatory-2: first 18 months of science data products, Atmos. Meas. Tech., 10, 549–563, https://doi.org/10.5194/amt-10-549-2017, 2017a.

Eldering, A., Wennberg, P. O., Crisp, D., Schimel, D. S., Gun- son, M. R., Chatterjee, A., Liu, J., Schwandner, F. M., Sun, Y., O'Dell, C. W., Frankenberg, C., Taylor, T., Fisher, B., Oster- man, G. B., Wunch, D., Hakkarainen, J., Tamminen, J., and Weir, B.: The Orbiting Carbon Observatory-2 early science investigations of regional carbon dioxide fluxes, Science, 358, eaam5745, https://doi.org/10.1126/science.aam5745, 2017b.

Feng, L., Palmer, P. I., Parker, R. J., Deutscher, N. M., Feist, D. G., Kivi, R., Morino, I., and Sussmann, R.: Estimates of European uptake of $CO_2$ inferred from GOSAT $XCO_2$ retrievals: Sensitivity to measurement bias inside and outside Europe. Atmos. Chem. Phys., 16, 1289–1302, https://doi.org/10.5194/acp-16-1289-2016, 2016.

Giglio, L., Randerson, J. T., and van der Werf, G. R.: Analysis of daily, monthly, and annual burned area using the fourth-generation global fire emissions database (GFED4) J. Geophys. Res. Biogeosci., 118, 317–328, https://doi.org/10.1002/jgrg.20042, 2013.

Griffith, D. W. T., Deutscher, N., Velazco, V. A., Wennberg, P. O., Yavin, Y., Keppel Aleks, G., Washenfelder, R., Toon, G. C., Blavier, J.-F., Murphy, C., Jones, N., Kettlewell, G., Connor, B., Macatangay, R., Roehl, C., Ryczek, M., Glowacki, J., Culgan, T., and Bryant, G.: TCCON data from Darwin, Australia, Release GGG2014R0. TCCON data archive, hosted by CaltechDATA, California Institute of Technology, Pasadena, CA, U.S.A. http://doi.org/10.14291/tccon.ggg2014.darwin01.R0/1149290, 2017a.

Griffith, D. W. T., Velazco, V. A., Deutscher, N., Murphy, C., Jones, N., Wilson, S., Macatangay, R., Kettlewell, G., Buchholz, R. R., and Riggenbach, M.: TCCON data from Wollongong, Australia, Release GGG2014R0. TCCON data archive, hosted by CaltechDATA, California Institute of Technology, Pasadena, CA, U.S.A. https://doi.org/10.14291/tccon.ggg2014.wollongong01.R0/1149291, 2017b.

Gurney, K. R., Law, R. M., Denning, A. S., Rayner, P. J., Baker, D., Bousquet, P., Bruhwiler, L., Chen, Y.-H., Ciais, P., Fan, S., Fung, I. Y., Gloor, M., Heimann, M., Higuchi, K., John, J., Maki, T., Maksyutov, S., Masarie, K., Peylin, P., Prather, M., Pak, B. C., Randerson, J., Sarmiento, J., Taguchi, S., Takahashi, T., and Yuen, C.-W.: Towards robust regional estimates of $CO_2$ sources and sinks using atmospheric transport models, Nature, 415, 626–630, 2002.

Henze, D. K., Hakami, A. and Seinfeld, J. H.: Development of the adjoint of GEOS-Chem, Atmos. Chem. Phys., 7, 2413-2433, 2007.

Heymann, J., Reuter, M., Buchwitz, M., Schneising, O., Bovens- mann, H., Burrows, J. P., Massart, S., Kaiser, J. W., and Crisp, D.: $CO_2$ emission of Indonesian fires in 2015 estimated from satellite-derived atmospheric $CO_2$ concentrations, Geophys. Res. Lett., 44, 1537–1544, https://doi.org/10.1002/2016GL072042, 2017.

Houweling, S., Breon, F.-M., Aben, I., R¨odenbeck, C., Gloor, M., Heimann, M., and Ciais, P.: Inverse modeling of $CO_2$ sources and sinks using satellite data: a synthetic inter-comparison of measurement techniques and their performance as a function of space and time, Atmos. Chem. Phys., 4, 523–538, https://doi.org/10.5194/acp-4-523-2004, 2004.

Houweling, S., Aben, I., Breon, F.-M., Chevallier, F., Deutscher, N., Engelen, R., Gerbig, C., Griffith, D., Hungershoefer, K., Macatangay, R., Marshall, J., Notholt, J., Peters, W., and Serrar, S.: The importance of transport model uncertainties for the estimation of $CO_2$ sources and sinks using satellite measurements, Atmos. Chem. Phys., 10, 9981–9992, https://doi.org/10.5194/acp-10-9981-2010, 2010.

Houweling, S., Baker, D., Basu, S., Boesch, H., Butz, A., Cheval- lier, F., Deng, F., Dlugokencky, E. J., Feng, L., Ganshin, A., Hasekamp, O., Jones, D., Maksyutov, S., Marshall, J., Oda, T., O'Dell, C. W., Oshchepkov, S., Palmer, P. I., Peylin, P., Poussi, Z., Reum, F., Takagi, H., Yoshida, Y., and Zhuravlev, R.: An intercomparison of inverse models for estimating sources and sinks of $CO_2$ using GOSAT measurements, J. Geophys. Res.-Atmos., 120, 5253–5266, https://doi.org/10.1002/2014JD022962, 2015.

Hungershoefer, K., Breon, F.-M., Peylin, P., Chevallier, F., Rayner, P., Klonecki, A., Houweling, S., and Marshall, J.: Evaluation of various observing systems for the global monitoring of $CO_2$ surface fluxes, Atmos. Chem. Phys., 10, 10503–10520, https://doi.org/10.5194/acp-10-10503-2010, 2010.

Jiang, Z., Jones, D. B. A., Kopacz, M., Liu, J., Henze, D. K., and Heald, C.: Quantifying the impact of model errors on top-down estimates of carbon monoxide emissions using satellite observations, J. Geophys. Res., 116, D15306, https://doi.org/10.1029/2010JD015282, 2011.

Kivi, R., Heikkinen, P., and Kyro, E.: TCCON data from Sodankyla, Finland, Release GGG2014R0. TCCON data archive, hosted by CaltechDATA, California Institute of Technology, Pasadena, CA, U.S.A. https://doi.org/10.14291/tccon.ggg2014.sodankyla01.R0/1149280, 2017.

Kopacz, M., Jacob, D. J., Henze, D. K., Heald, C. L., Streets, D. G., and Zhang, Q.: A comparison of analytical and adjoint Bayesian inversion methods for constraining Asian sources of CO using satellite (MOPITT) measurements of CO columns, J. Geophys. Res., 114, D04305, https://doi.org/10.1029/2007JD009264, 2009.

Kopacz, M., Jacob, D. J., Fisher, J. A., Logan, J. A., Zhang, L., Megretskaia, I. A, Yantosca, R. M., Singh, K., Henze, D. K., Burrows, J. P., Buchwitz, M., Khlystova, I., McMillan, W. W., Gille, J. C., Edwards, D. P., Eldering, A., Thouret, V., and Nedelec, P.: Global estimates of CO sources with high resolution by adjoint inversion of multiple satellite datasets (MOPITT, AIRS, SCIAMACHY, TES), Atoms. Chem. Phys., 10, 855-876, 2010.

Kuze, A., Suto, H., Nakajima, M., and Hamazaki, T.: Thermal and near infrared sensor for carbon observation Fourier-transform spectrometer on the Greenhouse Gases Observing Satellite for greenhouse gases monitoring. Appl. Opt., 48, 6716, https://doi.org/10.1364 /AO.48.006716, 2009.

Liu, J., Bowman, K. W., Lee, M., Henze, D. K., Bousserez, N., Brix, H., Collatz, G. J., Menemenlis, D., Ott, L., Pawson, S., Jones, D., and Nassar, R.: Carbon monitoring system flux estimation and attribution: impact of ACOS-GOSAT $XCO_2$ sampling on the inference of terrestrial biospheric sources and sinks, Tellus B, 66, 22486, https://doi.org/10.3402/tellusb.v66.22486, 2014.

Liu, J., Bowman, K. W., Schimel, D. S., Parazoo, N. C., Jiang, Z., Lee, M., Bloom, A. A., Wunch, D., Frankenberg, C., Sun, Y., O'Dell, C. W., Gurney, K. R., Menemenlis, D., Gierach, M., Crisp, D., and Eldering, A.: Contrasting carbon cycle responses of the tropical continents to the 2015–2016 El Niño, Science, 358, eaam5690, https://doi.org/10.1126/science.aam5690, 2017.

Maksyutov, S., Takagi, H., Valsala, V. K., Saito, M., Oda, T., Saeki, T., Belikov, D. A., Saito, R., Ito, A., Yoshida, Y., Morino, I., Uchino, O., Andres, R. J., and Yokota, T.: Regional $CO_2$ flux estimates for 2009–

2010 based on GOSAT and ground- based $CO_2$ observations, Atmos. Chem. Phys., 13, 9351–9373, https://doi.org/10.5194/acp-13-9351-2013, 2013.

Messerschmidt, J., Geibel, M. C., Blumenstock, T., Chen, H., Deutscher, N. M., Engel, A., Feist, D. G., Gerbig, C., Gisi, M., Hase, F., Katrynski, K., Kolle, O., Lavrič, J. V., Notholt, J., Palm, M., Ramonet, M., Rettinger, M., Schmidt, M., Sussmann, R., Toon, G. C., Truong, F., Warneke, T., Wennberg, P. O., Wunch, D., and Xueref-Remy, I.: Calibration of TCCON column-averaged $CO_2$: the first aircraft campaign over European TCCON sites, Atmos. Chem. Phys., 11, 10765-10777, https://doi.org/10.5194/acp-11-10765-2011, 2011.

Miller, C. E., Crisp, D., DeCola, P. L., Olsen, S. C., Randerson, J. T., Michalak, A. M., Alkhaled, A., Rayner, P., Jacob, D. J., Suntharalingam, P., Jones, D. B. A., Denning, A. S., Nicholls, M. E., Doney, S. C., Pawson, S., Boesch, H., Connor, B. J., Fung, I. Y., O'Brien, D., Salawitch, R. J., Sander, S. P., Sen, B., Tans, P., Toon, G. C.,Wennberg, P. O.,Wofsy, S. C., Yung, Y. L., and Law, R. M.: Precision requirements for space-based $XCO_2$ data, J. Geophys. Res., 112, D10314, https://doi.org/10.1029/2006JD007659, 2007.

Miller, S. M., Michalak, A. M., Yadav, V., and Tadić, J. M.: Characterizing biospheric carbon balance using $CO_2$ observations from the OCO-2 satellite, Atmos. Chem. Phys., 18, 6785-6799, https://doi.org/10.5194/acp-18-6785-2018, 2018.

Morino, I., Matsuzaki, T., and Shishime, A.: TCCON data from Tsukuba, Ibaraki, Japan, 125HR, Release GGG2014R2. TCCON data archive, hosted by CaltechDATA, California Institute of Technology, Pasadena, CA, U.S.A. http://doi.org/10.14291/tccon.ggg2014.tsukuba02.R2, 2017.

Nassar, R., Jones, D. B. A., Suntharalingam, P., Chen, J. M., Andres, R. J., Wecht, K. J., Yantosca, R. M., Kulawik, S. S., Bowman, K. W., Worden, J. R., Machida, T., and Matsueda, H.: Modeling global atmospheric $CO_2$ with improved emission inventories and $CO_2$ production from the oxidation of other carbon species, Geosci. Model Dev., 3, 689–716, https://doi.org/10.5194/gmd-3-689-2010, 2010.

Nassar, R., Hill, T. G., McLinden, C. A., Wunch, D., Jones, D. B. A., and Crisp, D.: Quantifying $CO_2$ emissions From Individual Power Plants from Space, Geophys. Res. Lett., 44, 10045– 10053, https://doi.org/10.1002/2017GL074702, 2017.

Notholt, J., Petri, C., Warneke, T., Deutscher, N., Buschmann, M., Weinzierl, C., Macatangay, R., and Grupe, P.: TCCON data from Bremen, Germany, Release GGG2014R0. TCCON data archive, hosted by CaltechDATA, California Institute of Technology, Pasadena, CA, U.S.A. https://doi.org/10.14291/tccon.ggg2014.bremen01.R0/1149275, 2017a.

Notholt, J., Schrems, O., Warneke, T., Deutscher, N., Weinzierl, C., Palm, M., Buschmann, M., and AWI-PEV Station Engineers: TCCON data from Ny Alesund, Spitzbergen, Norway, Release GGG2014R0. TCCON data archive, hosted by CaltechDATA, California Institute of Technology, Pasadena, CA, U.S.A. https://doi.org/10.14291/tccon.ggg2014.nyalesund01.R0/1149278, 2017b.

ObsPack: Cooperative Global Atmospheric Data Integration Project, Multi-laboratory compilation of atmospheric carbon dioxide data for the period 1957–2015, obspack_co2_1_GLOBALVIEWplus_v2.1_2016-09-02, NOAA Earth System Research Laboratory, Global Monitoring Division, https://doi.org/10.15138/G3059Z, 2016.

O'Dell, C., Connor, B., Bösch, H., O'Brien, D., Frankenberg, C., Castano, R., Christi, M., Eldering, D., Fisher, B., Gunson, M., McDuffie, J., Miller, C. E., Natraj, V., Oyafuso, F., Polonsky, I., Smyth, M., Taylor, T., Toon, G., Wennberg, P., and Wunch, D.: The ACOS $CO_2$ retrieval algorithm – Part 1: Description and validation against synthetic observations, Atmos. Meas. Tech., 5, 99-121, https://doi.org/10.5194/amt-5-99-2012, 2012.

Oda, T. and Maksyutov, S. 2011. A very high-resolution (1 km x 1 km) global fossil fuel $CO_2$ emission inventory derived using a point source database and satellite observations of nighttime lights. *Atmos. Chem. Phys.* 11, 543 – 556.

Park, B. C. and Prather, M. J.: $CO_2$ source inversions using satellite observations of the upper troposphere,

Geophys. Res. Lett., 28, 4571–4574, https://doi.org/10.1029/2001GL013604, 2001.

Parrington, M., Palmer, P. I., Henze, D. K., Tarasick, D. W., Hyer, E. J., Owen, R. C., Clerbaux, C., Bowman, K. W., Deeter, M. N., Barratt, E. M., Coheur, P.-F., Hurtmans, D., George, M., and Worden, J. R.: The influence of boreal biomass burning emissions on the distribution of tropospheric ozone over North America and the North Atlantic during 2010, Atmos. Chem. Phys., 12, 2077-2098, 2012.

Patra, P. K., Crisp, D., Kaiser, J. W., Wunch, D., Saeki, T., Ichii, K., Sekiya, T., Wennberg, P. O., Feist, D. G., Pollard, D. F., Griffith, D. W. T., Velazco, V. A., De Maziere, M., Sha, M. K., Roehl, C., Chatterjee, A., and Ishijima, K.: The Orbiting Carbon Observa- tory (OCO-2) tracks 2–3 peta-gram increase in carbon release to the atmosphere during the 2014–2016 El Niño, Sci. Rep.-UK, 7, 13567, https://doi.org/10.1038/s41598-017-13459-0, 2017.

Peters, W., Jacobson, A. R., Sweeney, C., Andrews, A. E., Conway, T. J., Masarie, K., Miller, J. B., Bruhwiler, L. M. P., P´etron, G., Hirsch, A. I.,Worthy, D. E. J.,Werf, G. R. V. D., Randerson, J. T., Wennberg, P. O., Krol, M. C., and Tans, P. P.: An atmospheric perspective on North American carbon dioxide exchange: CarbonTracker, P. Natl. Acad. Sci., 104, 18925–18930, 2007..

Peylin, P., Law, R. M., Gurney, K. R., Chevallier, F., Jacobson, A. R., Maki, T., Niwa, Y., Patra, P. K., Peters, W., Rayner, P. J., Rödenbeck, C., van der Laan-Luijkx, I. T., and Zhang, X.: Global atmospheric carbon budget: results from an ensemble of atmospheric $CO_2$ inversions, Biogeosciences, 10, 6699–6720, https://doi.org/10.5194/bg-10-6699-2013, 2013.

Potter, C. S., Randerson, J. T., Field, C. B., Matson, P. A., Vitousek, P. M., Mooney, H. A., and Klooster, S. A.: Terrestrial ecosystem production: A process model based on global satellite and surface data, Global Biogeochem. Cycles, 7(4), 811–841, https://doi.org/10.1029/93GB02725, 1993.

Rayner, P. J. and O'Brien, D. M.: The utility of remotely sensed $CO_2$ concentration data in surface source inversions, Geophys. Res. Lett., 28, 175–178, https://doi.org/10.1029/2000GL011912, 2001.

Reuter, M., Buchwitz, M., Hilker, M., Heymann, J., Schneising, O., Pillai, D., Bovensmann, H., Burrows, J. P., Bösch, H., Parker, R., Butz, A., Hasekamp, O., O'Dell, C. W., Yoshida, Y., Gerbig, C., Nehrkorn, T., Deutscher, N. M., Warneke, T., Notholt, J., Hase, F., Kivi, R., Sussmann, R., Machida, T., Matsueda, H., and Sawa, Y.: Satellite-inferred European carbon sink larger than expected, Atmos. Chem. Phys., 14, 13739-13753, https://doi.org/10.5194/acp-14-13739-2014, 2014.

Reuter, M., Buchwitz, M., Hilker, M., Heymann, J., Bovensmann, H., Burrows, J. P., Houweling, S., Liu, Y. Y., Nassar, R., Chevallier, F., Ciais, P., Marshall, J., and Reichstein, M.: How Much $CO_2$ Is Taken Up by the European Terrestrial Biosphere?. Bull. Amer. Meteor. Soc., 98, 665–671, https://doi.org/10.1175/BAMS-D-15-00310.1, 2017.

Rienecker, M. M., Suarez, M. J., Todling, R., Bacmeister, J., Takacs, L. and co-authors: The GEOS-5 Data Assimilation System-Documentation of versions 5.0.1 and 5.1.0, and 5.2.0 NASA Tech. Rep. Series on Global Modeling and Data Assimilation, NASA/TM-2008-104606, Vol. 27, 92 pp, 2008.

Rodgers, C. D.: Inverse Methods for Atmospheric Sounding: Theory and Practice, World Scientific Publishing Co Inc, Singapore, chapter 2, 2000.

Saeki, T., Maksyutov, S., Saito, M., Valsala, V., Oda, T., An- dres, R. J., Belikov, D., Tans, P., Dlugokencky, E., Yoshida, Y., Morino, I., Uchino, O., and Yokota, T.: Inverse modeling of $CO_2$ fluxes using GOSAT data and multi-year ground-based obser- vations, SOLA, 9, 45–50, https://doi.org/10.2151/sola.2013-011, 2013.

Sherlock, V., Connor, B., Robinson, J., Shiona, H., Smale, D., and Pollard, D.: TCCON data from Lauder, New Zealand, 125HR, Release GGG2014R0. TCCON data archive, hosted by CaltechDATA, California Institute of Technology, Pasadena, CA, U.S.A. https://doi.org/10.14291/tccon.ggg2014.lauder02.R0/1149298, 2017.

Singh, K., Jardak, M., Sandu, A., Bowman, K., Lee, M., and Jones, D.: Construction of non-diagonal background error covariance matrices for global chemical data assimilation, Geosci. Model Dev., 4, 299-316, https://doi.org/10.5194/gmd-4-299-2011, 2011.

Suntharalingam, P., Jacob, D. J., Palmer, P. I., Logan, J. A., Yantosca, R. M. and co-authors: Improved quantification of Chinese carbon fluxes using $CO_2$/CO correlations in Asian outflow. J. Geophys. Res. 109, D18S18, https://doi.org/10.1029/2003JD004362, 2004.

Sussmann, R., and Rettinger, M.: TCCON data from Garmisch, Germany, Release GGG2014R2. TCCON data archive, hosted by CaltechDATA, California Institute of Technology, Pasadena, CA, U.S.A. https://doi.org/10.14291/tccon.ggg2014.garmisch01.R2, 2017.

Tarantola, A.: Inverse Problem Theory and Methods for Model Parameter Estimation, Soc. Industr. App.l Math., Philadelphia, PA, USA, 2004.

van der Werf, G. R., Randerson, J. T., Giglio, L., Collatz, G. J., Mu, M., Kasibhatla, P. S., Morton, D. C., DeFries, R. S., Jin, Y., and van Leeuwen, T. T.: Global fire emissions and the contribution of deforestation, savanna, forest, agricultural, and peat fires (1997–2009), Atmos. Chem. Phys., 10, 11707–11735, https://doi.org/10.5194/acp-10-11707-2010, 2010.

Wang, X., Guo, Z., Huang, Y. P., Fan, H. J., and Li, W. B.: A cloud detection scheme for the Chinese carbon dioxide observation satellite (TANSAT). Adv. Atmos. Sci., 34(1), 16–25, https://doi.org/10.1007/s00376-016-6033-y, 2017.

Warneke, T., Messerschmidt, J., Notholt, J., Weinzierl, C., Deutscher, N., Petri, C., Grupe, P., Vuillemin, C., Truong, F., Schmidt, M., Ramonet, M., and Parmentier, E.: TCCON data from Orleans, France, Release GGG2014R0. TCCON data archive, hosted by CaltechDATA, California Institute of Technology, Pasadena, CA, U.S.A. https://doi.org/10.14291/tccon.ggg2014.orleans01.R0/1149276, 2017.

Wennberg, P. O., Roehl, C., Wunch, D., Toon, G. C., Blavier, J.-F., Washenfelder, R., Keppel-Aleks, G., Allen, N., and Ayers, J.: TCCON data from Park Falls, Wisconsin, USA, Release GGG2014R1. TCCON data archive, hosted by CaltechDATA, California Institute of Technology, Pasadena, CA, U.S.A. http://doi.org/10.14291/tccon.ggg2014.parkfalls01.R1, 2017.

Wennberg, P. O., Wunch, D., Roehl, C., Blavier, J.-F., Toon, G. C., Allen, N., Dowell, P., Teske, K., Martin, C., and Martin, J.: TCCON data from Lamont, Oklahoma, USA, Release GGG2014R1. TCCON data archive, hosted by CaltechDATA, California Institute of Technology, Pasadena, CA, U.S.A. https://doi.org/10.14291/tccon.ggg2014.lamont01.R1/1255070, 2017. Wilkerson, J. T., Jacobson, M. Z., Malwitz, A., Balasubramanian, S., Wayson, R., Fleming, G., Naiman, A. D., and Lele, S. K.: Analysis of emission data from global commercial aviation: 2004 and 2006, Atmos. Chem. Phys., 10, 6391-6408, https://doi.org/10.5194/acp-10-6391-2010, 2010.

Wunch, D., Toon, G. C., Wennberg, P. O., Wofsy, S. C., Stephens, B. B., Fischer, M. L., Uchino, O., Abshire, J. B., Bernath, P., Biraud, S. C., Blavier, J.-F. L., Boone, C., Bowman, K. P., Browell, E. V., Campos, T., Connor, B. J., Daube, B. C., Deutscher, N. M., Diao, M., Elkins, J. W., Gerbig, C., Gottlieb, E., Griffith, D. W. T., Hurst, D. F., Jimenez, R., Keppel-Aleks, G., Kort, E. A., Macatangay, R., Machida, T., Matsueda, H., Moore, F., Morino, I., Park, S., Robinson, J., Roehl, C. M., Sawa, Y., Sherlock, V., Sweeney, C., Tanaka, T., and Zondlo, M. A.: Calibration of the Total Carbon Column Observing Network using aircraft profile data, Atmos. Meas. Tech., 3, 1351-1362, doi:10.5194/amt-3-1351-2010, 2010.

Wunch, D., Wennberg, P. O., Toon, G. C., Connor, B. J., Fisher, B., Osterman, G. B., Frankenberg, C., Mandrake, L., O'Dell, C., Ahonen, P., Biraud, S. C., Castano, R., Cressie, N., Crisp, D., Deutscher, N. M., Eldering, A., Fisher, M. L., Griffith, D. W. T., Gunson, M., Heikkinen, P., Keppel-Aleks, G., Kyrö, E., Lindenmaier, R., Macatangay, R., Mendonca, J., Messer- schmidt, J., Miller, C. E., Morino, I., Notholt, J., Oyafuso, F. A., Rettinger, M., Robinson, J., Roehl, C. M., Salawitch, R. J., Sherlock, V., Strong, K., Sussmann, R., Tanaka, T., Thomp- son, D. R., Uchino, O., Warneke, T., and Wofsy, S. C.: A method for evaluating bias in global measurements of $CO_2$ total columns from space, Atmos. Chem. Phys., 11, 12317–12337, https://doi.org/10.5194/acp-11-12317-2011, 2011.

Wunch, D., Wennberg, P. O., Osterman, G., Fisher, B., Naylor, B., Roehl, C. M., O'Dell, C., Mandrake, L., Viatte, C., Kiel, M., Griffith, D. W. T., Deutscher, N. M., Velazco, V. A., Notholt, J., Warneke, T., Petri, C., De Maziere, M., Sha, M. K., Sussmann, R., Rettinger, M., Pollard, D., Robinson, J., Morino, I., Uchino, O., Hase, F., Blumenstock, T., Feist, D. G., Arnold, S. G., Strong, K., Mendonca, J., Kivi, R.,

Heikkinen, P., Iraci, L., Podolske, J., Hillyard, P. W., Kawakami, S., Dubey, M. K., Parker, H. A., Sepulveda, E., García, O. E., Te, Y., Jeseck, P., Gunson, M. R., Crisp, D., and Eldering, A.: Comparisons of the Orbiting Carbon Observatory-2 (OCO-2) $XCO_2$ measurements with TCCON, At- mos. Meas. Tech., 10, 2209–2238, https://doi.org/10.5194/amt- 10-2209-2017, 2017.

Yang, D. X., Liu, Y., Cai, Z. N., Chen, X., Yao, L., and Lu, D. R.: First global carbon dioxide maps produced from TanSat measurements. Adv. Atmos. Sci., 35(6), 621–623, https://doi.org/10.1007/s00376-018-7312-6, 2018.

Zhu, C., Byrd, R. H., Lu, P. and Nocedal, J.: L-BFGS-B: algorithm 778: L-BFGS-B, FORTRAN routines for large scale bound constrained optimization. ACM Trans. Math. Softw. 23(4), 550_560. https://doi.org/10.1145/279232.279236, 1997.